Article

Current Biology

Force-induced dephosphorylation activates the cochaperone BAG3 to coordinate protein homeostasis and membrane traffic

Graphical abstract

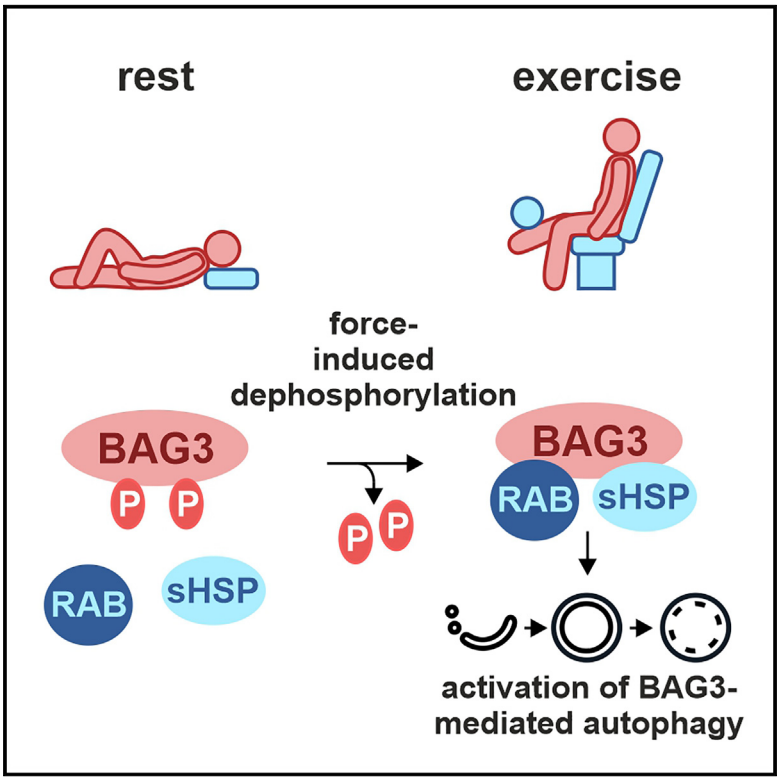

Highlights

- Mechanical forces trigger BAG3 dephosphorylation in human muscle and isolated cells
- BAG3 dephosphorylation stimulates binding to sHSPs and RAB GTPases to activate CASA
- RAB7A and RAB11B are essential for CASA in skeletal muscle cells
- RAB7A-L129F overactivates CASA in Charcot-Marie-Tooth patient cells

Authors

Judith Ottensmeyer, Alessandra Esch, Henrique Baeta, ..., Vincent Timmerman, Pitter F. Huesgen, Jörg Höhfeld

Correspondence

hoehfeld@uni-bonn.de

In brief

The protein BAG3 is essential for maintaining skeletal and cardiac muscles. Ottensmeyer et al. show that force-induced dephosphorylation triggers the association of BAG3 with molecular chaperones and membrane trafficking factors to promote the autophagic degradation of damaged proteins under stress conditions.

Ottensmeyer et al., 2024, Current Biology *34*, 1–14
September 23, 2024
https://doi.org/10.1016/j.cub.2024.07.088

CellPress

Current Biology

CellPress
OPEN ACCESS

Article

Force-induced dephosphorylation activates the cochaperone BAG3 to coordinate protein homeostasis and membrane traffic

Judith Ottensmeyer,[1,9] Alessandra Esch,[1,9] Henrique Baeta,[2,9] Sandro Sieger,[1] Yamini Gupta,[1] Maximilian F. Rathmann,[1] Andreas Jeschke,[1] Daniel Jacko,[3] Kirill Schaaf,[3] Thorsten Schiffer,[4] Bahareh Rahimi,[5] Lukas Lövenich,[5] Angela Sisto,[6] Peter F.M. van der Ven,[1] Dieter O. Fürst,[1] Albert Haas,[1] Wilhelm Bloch,[3] Sebastian Gehlert,[3,7] Bernd Hoffmann,[5] Vincent Timmerman,[6] Pitter F. Huesgen,[2,8] and Jörg Höhfeld[1,10,*]

[1]Institute for Cell Biology, University of Bonn, Ulrich-Haberland-Str. 61a, 53121 Bonn, Germany
[2]Institute for Biology II, University of Freiburg, Schänzlestraße 1, 79104 Freiburg, Germany
[3]Institute of Cardiovascular Research and Sports Medicine, German Sport University, Am Sportpark Müngersdorf 6, 50933 Cologne, Germany
[4]Outpatient Clinic for Sports Traumatology, German Sport University, Am Sportpark Müngersdorf 6, 50933 Cologne, Germany
[5]Institute of Biological Information Processing, Forschungszentrum Jülich, Wilhelm-Johnen-Straße, 52428 Jülich, Germany
[6]Peripheral Neuropathy Research Group, Department of Biomedical Sciences, Institute Born Bunge and University of Antwerp, Universiteitsplein 1, 2610 Antwerp, Belgium
[7]Institute of Sport Science, University of Hildesheim, Universitätsplatz 1, 31139 Hildesheim, Germany
[8]CIBSS - Centre for Integrative Biological Signaling Studies, University of Freiburg, Schänzlestr. 18, 79104 Freiburg, Germany
[9]These authors contributed equally
[10]Lead contact
*Correspondence: hoehfeld@uni-bonn.de
https://doi.org/10.1016/j.cub.2024.07.088

SUMMARY

Proteome maintenance in contracting skeletal and cardiac muscles depends on the chaperone-regulating protein BAG3. Reduced BAG3 activity leads to muscle weakness and heart failure in animal models and patients. BAG3 and its chaperone partners recognize mechanically damaged muscle proteins and initiate their disposal through chaperone-assisted selective autophagy (CASA). However, molecular details of the force-dependent regulation of BAG3 have remained elusive so far. Here, we demonstrate that mechanical stress triggers the dephosphorylation of BAG3 in human muscle and in isolated cells. We identify force-regulated phospho-switches in BAG3 that control CASA complex assembly and CASA activity. Differential proteomics reveal RAB GTPases, which organize membrane traffic and fusion, as dephosphorylation-dependent interactors of BAG3. In fact, RAB7A and RAB11B are shown here to be essential for CASA in skeletal muscle cells. Moreover, BAG3 dephosphorylation is also observed upon induction of mitophagy, suggesting an involvement of the cochaperone in the RAB7A-dependent autophagic engulfment of damaged mitochondria in exercised muscle. Cooperation of BAG3 with RAB7A relies on a direct interaction of both proteins, which is regulated by the nucleotide state of the GTPase and by association with the autophagosome membrane protein LC3B. Finally, we provide evidence that BAG3 and RAB7A also cooperate in non-muscle cells and propose that overactivation of CASA in RAB7A-L129F patients contributes to the loss of peripheral neurons in Charcot-Marie-Tooth neuropathy.

INTRODUCTION

Cellular protein homeostasis (proteostasis) under biotic and abiotic stress depends on a cooperation of molecular chaperones with protein degradation systems.[1,2] Stress-unfolded proteins are recognized by chaperones, which mediate refolding to the native state whenever possible. However, in case of irreversible damage, chaperones cooperate with degradation factors for client protein disposal through the ubiquitin-proteasome-system or autophagy pathways.[1] During chaperone-assisted selective autophagy (CASA), client recognition is facilitated by the BCL2-associated athanogene 3 (BAG3), which links chaperones of the 70-kDa heat shock protein (HSP70) family to small heat shock proteins (sHSPs).[3,4] Following client ubiquitylation by a chaperone-associated ubiquitin ligase and recruitment of autophagic ubiquitin receptors, the CASA-client complex is engulfed by phagophore membranes, leading to autophagosome (AP) formation and ultimately to degradation in autolysosomes (ALs).[3] In neurons, CASA mediates the degradation of aggregation-prone proteins linked to neurodegeneration. This includes the microtubule-associated protein tau, which accumulates in Alzheimer's disease, and mutant variants of SOD1 and Huntingtin that form aggregates in brains of amyotrophic lateral sclerosis (ALS) and Huntington's disease patients, respectively.[5–8] In mechanically

Please cite this article in press as: Ottensmeyer et al., Force-induced dephosphorylation activates the cochaperone BAG3 to coordinate protein homeostasis and membrane traffic, Current Biology (2024), https://doi.org/10.1016/j.cub.2024.07.088

stressed cells, CASA degrades the actin-crosslinking protein filamin following force-induced unfolding and damage.[9–12] Disposal of damaged filamin is necessary for maintaining the integrity of the sarcomere, the smallest contractile unit of striated muscle.[9–13] In fact, mutations in BAG3 cause rapidly progressing muscle dystrophy and cardiomyopathy in animal models and patients.[12,14–18] Moreover, a reduction of BAG3 activity contributes to heart failure,[11] which is a leading cause of morbidity and mortality in industrialized countries, affecting 64 million people worldwide.[19] Evidently, BAG3 expression and activity need to be carefully adjusted to stress levels to ensure cell survival and tissue homeostasis. In human skeletal muscle, BAG3 expression is indeed upregulated following resistance exercise (RE) to cope with cytoskeleton damage.[20] In this situation, accumulation of force-unfolded proteins is sensed by HSP70 chaperones, resulting in the activation of the heat shock transcription factor 1 (HSF1), which in turn triggers *BAG3* transcription.[9,21] Besides transcriptional regulation, recent studies also point to an adaptive modulation of BAG3 activity through posttranslational modification.[22,23] In line with this, proteomic analysis of the phospho-proteome of exercised human muscle and contracting mouse muscle revealed significant changes of the phosphorylation status of BAG3 compared to resting muscle.[24–26] However, functional consequences remained elusive so far. Here, we show that BAG3 is dephosphorylated on multiple residues in response to mechanical forces that are externally applied to cells or internally generated. We identify phospho-switches in BAG3, which control its cooperation with sHSPs during client recognition and sequestration and with autophagy-stimulating membrane trafficking factors during CASA execution. The findings shed light on critical regulatory steps of BAG3-mediated proteostasis, which could be explored for therapeutic intervention in pathologies caused by BAG3 dysfunction.

RESULTS

BAG3 is subjected to force-induced dephosphorylation

Available proteomic data reveal extensive changes of the phosphorylation status of BAG3 in human and murine muscle following exercise and electrical stimulation.[24–26] Notably, most of the regulated phosphosites display reduced levels of phosphorylation under mechanical stress, suggesting that force-induced dephosphorylation could activate BAG3-mediated proteostasis (Figure 1A).

We succeeded in generating a phospho-specific antibody against one of the force-regulated sites, i.e., serine-136 of human BAG3 (Figures 1A and S1). It is the terminal serine of the first arginine-serine-glutamine-serine (RSQS) motif of the cochaperone, which mediates binding of BAG3 to 14-3-3 proteins during the microtubule-dependent transport of misfolded proteins to perinuclear aggresomes.[22] Using the phospho-specific antibody, significant dephosphorylation of BAG3 was observed in vastus lateralis muscle biopsies of unadapted human subjects after standardized mechanical overload (SMO1; R1 and E1) (Figures 1B and 1C). Moreover, SMO-induced dephosphorylation of BAG3 was attenuated following an adaptation phase with repeated bouts of RE (SMO2; R2 and E2). Repeated training reduces force-induced damage of sarcomeric proteins[20] and hence diminishes a requirement for BAG3 activation. The data confirm that BAG3 is dephosphorylated in exercised human muscle and illustrate an inverse correlation between BAG3 dephosphorylation and the training status of the subject.

BAG3 dephosphorylation was also monitored in C2C12 mouse myotubes, in which twitch contractions were induced by electrical pulse stimulation (EPS). EPS mimics exercise regimens in humans with high intensities leading to comparable damage in muscle cytoskeleton architecture.[27] Of note, applying EPS of increasing intensity to mouse myotubes caused increasing dephosphorylation of BAG3 (Figure 1D).

Finally, A7r5 rat smooth muscle cells were grown on elastomer substrates and subjected to unidirectional cyclic stretch. In this experimental setup, cells respond to the applied force with a reorientation of their actin cytoskeleton perpendicular to the force axis to minimize strain.[28] Reorientation occurs in a BAG3 and autophagy-dependent manner within 4 h of stretching.[28] Strikingly, cyclic stretch resulted in a strong dephosphorylation of BAG3 within the first hour of treatment, before phosphorylation returned to control level at 4 h (Figure 1E). Dephosphorylation of the cochaperone is apparently an immediate response to applied strain that is reversed when cells adapt through cytoskeleton reorientation.

Taken together, the dephosphorylation of BAG3 emerges as a common physiological response to internally generated and externally applied mechanical forces in mammalian cells.

Dephosphorylation of BAG3 stimulates CASA complex formation and activates CASA

To elucidate functional consequences of BAG3 dephosphorylation, we mutated serine and threonine residues of human BAG3, which were identified to be dephosphorylated in exercised human muscle,[24] namely S136, S264, S275, S279, T285, and S289 (Figure 1A). Residues were exchanged to alanine (A) and aspartic acid (D) to mimic the dephosphorylated and phosphorylated state, respectively (Figure 2A). In initial experiments, the impact of these mutations on CASA complex formation was investigated. HeLa cells were chosen for this approach because they are readily transfected, and CASA complex formation is well detectable in these cells.[12] FLAG-tagged phosphosite mutant variants of BAG3 were transiently expressed in HeLa cells, followed by immunoprecipitation and complex analysis (Figure 2A). Phosphorylation mimicry at single sites did not affect association of BAG3 with its chaperone partners HSPB8 and the constitutively expressed HSP70 protein heat shock cognate 70 (HSC70) (Figures S2A–S2F). Yet, when amino acid exchanges at position T285 and S289 were combined, CASA complex formation was affected (Figures 2B and 2C). The mutant variant that represents the dephosphorylated state (T285A/S289A) behaved like wild-type BAG3 and interacted with HSPB8 and HSC70 (Figures 2B and 2C). In contrast, phosphorylation mimicry on both residues (T285D/S289D) reduced binding to HSPB8. Force-induced dephosphorylation of BAG3 apparently triggers a transition from a core BAG3/HSC70 complex, which prevails under rest, to the fully assembled CASA complex with incorporated HSPB8.

To investigate how BAG3 phosphosite mutant variants affect CASA activity, the degradation of the BAG3 interactor SYNPO2 was analyzed in A7r5 smooth muscle cells. In this cell

Please cite this article in press as: Ottensmeyer et al., Force-induced dephosphorylation activates the cochaperone BAG3 to coordinate protein homeostasis and membrane traffic, Current Biology (2024), https://doi.org/10.1016/j.cub.2024.07.088

CellPress
OPEN ACCESS

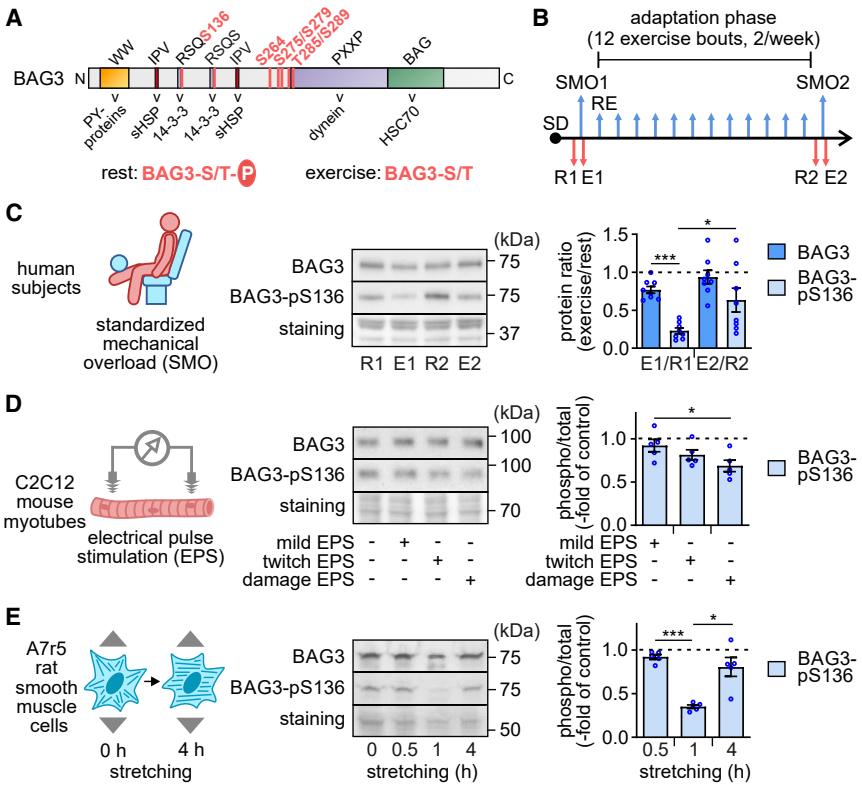

Figure 1. BAG3 is dephosphorylated in response to mechanical forces

(A) Schematic presentation of the domain structure of human BAG3 with domain-interacting proteins indicated below. Residues, which were identified by Hoffman et al.[24] as being subjected to exercise-induced dephosphorylation in human muscle, are shown in red. WW, tryptophan-containing domain that mediates binding to PY-motif-containing partner proteins; IPV, isoleucine-proline-valine motif that mediates binding to sHSPs; RSQS, arginine-serine-glutamine-serine motif that mediates binding to 14-3-3 proteins; PXXP, proline-x-x-proline motif that mediates binding to dynein; BAG, BCL2-associated athanogene signature domain that mediates binding to HSC70.

(B) Overview of the human study design. Following strength diagnostics (SDs), human subjects performed standardized mechanical overload (SMO1, unadapted state) and resistance exercise (RE) as indicated. After an adaptation phase with 12 exercise bouts, subjects performed a second SMO (SMO2, adapted state). Biopsies were taken 4 days before (rest: R1 and R2) and 60 min after SMO (exercise: E1 and E2).

(C) BAG3 and phosphorylated BAG3 (BAG3-pS136) were detected in lysates from muscle biopsies taken before (R1 and E1) and after an adaptation phase with repetitive RE sessions (R2 and E2). Staining reflects protein detection on blot membranes by Ponceau S. Protein levels were quantified from 8 human subjects, and protein ratios between exercise and rest were calculated. The dashed line indicates a ratio of 1 with no change between exercise and rest. Data are shown as mean values for E/R ratios ± SEM, $n = 8$.

(D) Differentiated C2C12 myotubes were subjected to electrical pulse stimulation (EPS) of increasing intensity for 5 h, followed by detection of BAG3 and BAG3-pS136 with specific antibodies. Protein levels were quantified, and the ratio between BAG3-pS136 and total BAG3 (phospho/total) observed in untreated control cells was set to 1. The dashed line represents the control value. Data are shown as mean values ± SEM, $n = 5$.

(E) A7r5 rat smooth muscle cells were subjected to unidirectional cyclic stretch at 0.3 Hz and 20% amplitude for 4 h. At 0, 0.5, 1, and 4 h cells were collected and analyzed for BAG3 and BAG3-pS136 levels. Protein levels were quantified, and the ratio between BAG3-pS136 and total BAG3 (phospho/total) observed in untreated control cells was set to 1. The dashed line represents the control value. Data are shown as mean values ± SEM, $n = 5$.

Statistical analysis was carried out using two-tailed unpaired t test with Welch's correction: $^{*}p < 0.05$, $^{***}p < 0.001$.

See also Figure S1.

line, CASA is active when intracellular tension is generated upon cultivation on the extracellular matrix protein fibronectin.[9] To monitor degradation, cells were treated with the translation inhibitor cycloheximide, and the reduction of the cellular concentration of SYNPO2 isoforms was followed by immunoblot analysis (Figures 2D and 2E). SYNPO2 links the CASA machinery to a membrane fusion complex, which facilitates engulfment by AP membranes.[9] SYNPO2 is, therefore, co-degraded during CASA. Consistent with previous data,[9] SYNPO2 isoforms were turned over with a half-life of about 3 h in A7r5 cells (Figure 2E). Expression of wild-type BAG3 or dephosphorylation-mimicking alanine variants did not significantly affect SYNPO2 degradation. However, T285D/S289D, T285D, and S136D mutant variants, which mimic phosphorylation of these sites, acted as dominant-negative proteins and abrogated SYNPO2 turnover (Figure 2E). CASA regulating activity was specific for these residues, as D variants of residues S264, S275, S279, or S289 did not interfere with SYNPO2 degradation (Figures S2G and S2H). In conclusion, force-induced dephosphorylation of S136, T285, and T285/S289 activates the CASA degradation pathway under mechanical stress.

BAG3 associates with RAB GTPases in a dephosphorylation-dependent manner

To explore the molecular basis of the observed dephosphorylation-dependent activation of CASA, differential interaction proteomics of BAG3 phosphosite mutant variants was performed. A and D variants of S136, T285, and T285/S289 were expressed in A7r5 cells as FLAG-tagged fusion proteins followed by anti-FLAG immunoprecipitation and mass spectrometry (Figure 3A). Whereas dephosphorylation mimicry at position S136 did not significantly stimulate binding of BAG3 to partner proteins (Table S1), the interactomes of T285 and T285/S289 mutant variants were significantly affected (Figures 3B, 3C, 3E, and S3F) (Data S1 and S2). In agreement with findings for HeLa cells (Figures 2B and 2C), BAG3-T285A/S289A displayed increased binding to sHSPs compared with the T285D/S289D variant when expressed in A7r5 smooth muscle cells (Figure 3B). Yet, instead of HSPB8, HSPB1 was detected in BAG3 complexes isolated from this cell type. HSPB1 is another member of the sHSP family, which interacts with BAG3[29] and contributes to muscle proteostasis.[30] Indeed, HSPB8 is not expressed in A7r5 smooth muscle cells (Figure S3A), suggesting that HSPB1 replaces

Please cite this article in press as: Ottensmeyer et al., Force-induced dephosphorylation activates the cochaperone BAG3 to coordinate protein homeostasis and membrane traffic, Current Biology (2024), https://doi.org/10.1016/j.cub.2024.07.088

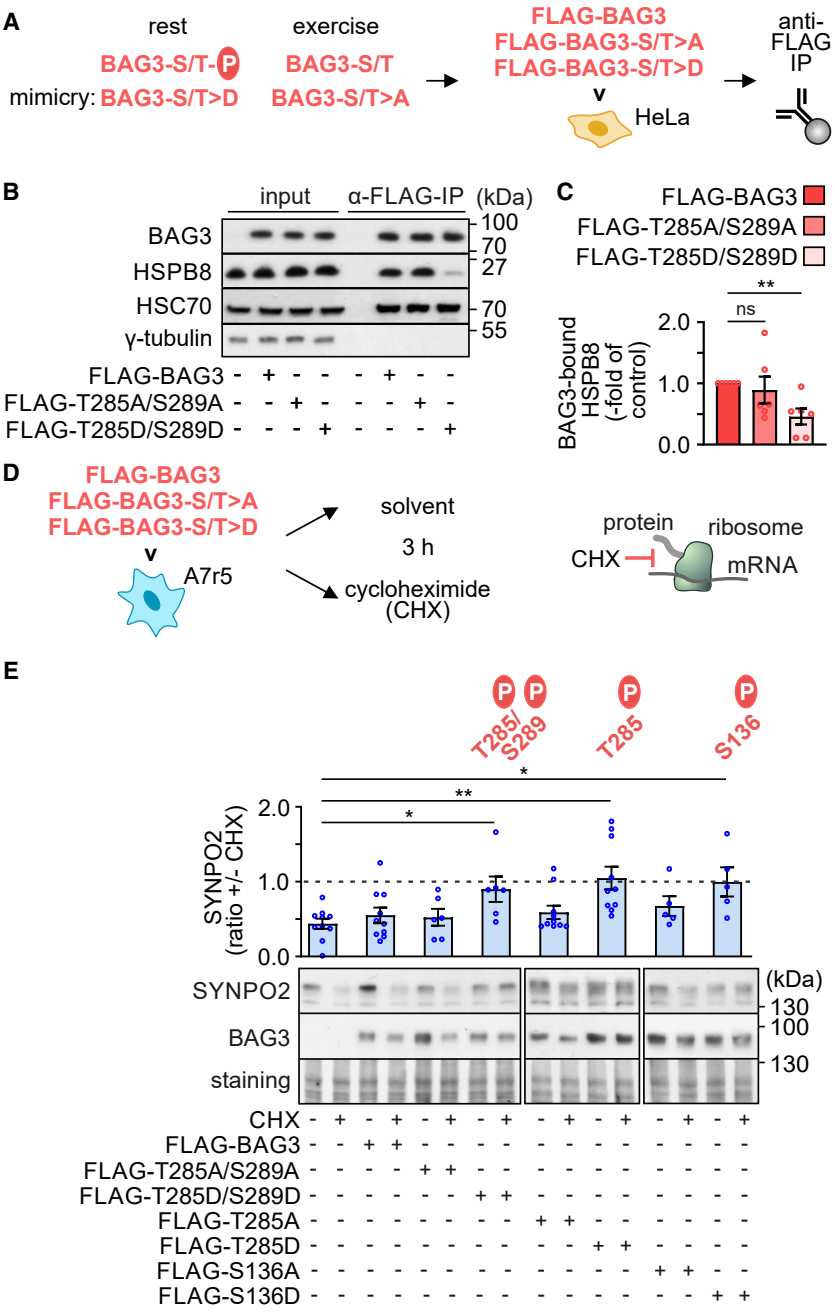

Figure 2. BAG3 phosphosite mutant variants that mimic the phosphorylated state interfere with CASA complex formation and CASA activity

(A) Phosphosite mutant variants of BAG3 were designed to mimic the different states of BAG3 and were transiently expressed in HeLa cells as FLAG-epitope tagged proteins followed by anti-FLAG immunoprecipitation.

(B) Immunoprecipitated complexes were probed with specific antibodies for the presence of BAG3, HSPB8, and HSC70.

(C) Data obtained under (B) were quantified with levels for HSPB8 detected in complexes of wild-type BAG3 (FLAG-BAG3) set to 1. Data are shown as mean values ± SEM, $n = 5$.

(D) BAG3 and BAG3 phosphosite mutant variants were transiently expressed in A7r5 rat smooth muscle cells cultivated on fibronectin. 48 h after transfection, cells were treated with cycloheximide (CHX) for 3 h to block protein synthesis.

(E) Lysates of A7r5 cells that recombinantly express the indicated proteins were prepared and subjected to western blot analysis using antibodies against SYNPO2 and BAG3. SYNPO2 is detectable as multiple isoforms in this cell type. Levels of SYNPO2 were quantified, and the ratio of levels in the presence of CHX or the solvent DMSO was determined (ratio ± CHX). The dashed line represents a ratio of 1 with no changes upon CHX treatment. Data are shown as mean values ± SEM, $n \geq 5$.

Statistical analysis was carried out using two-tailed unpaired t test with Welch's correction: $^{*}p < 0.05$; $^{**}p < 0.01$; ns, non-significant.

See also Figure S2.

HSPB8 in this cell type. In agreement with this, HSPB1 depletion abrogated the autophagic degradation of BAG3 in A7r5 cells (Figures S3B and S3C). HSPB1 was also detected in BAG3-T285A complexes (Figure S3C). However, different from the double-mutant variant BAG3-T285D/S289D, exchange of threonine-285 to aspartic acid alone (BAG3-T285D) did not significantly reduce HSPB1 binding. Again, this is consistent with observations from HeLa cells (Figures 2B, 2C, and S2E) and illustrates that multisite dephosphorylation on T285 and S289 is required to facilitate an interaction of BAG3 with HSPB1 and HSPB8.

Gene Ontology (GO) term analysis of BAG3-associated proteins showed an enrichment of cytoskeleton, chaperone, and ubiquitin ligase-binding proteins, consistent with the proteostasis function of BAG3 in cytoskeleton maintenance (Figures 3D and S3E). Moreover, several nucleotide triphosphate hydrolases, e.g., GTPases, were detected in BAG3 complexes. The small GTPases RAB7A and RAB11A/B were significantly enriched in BAG3-T285A/S289A complexes compared to those of the double aspartic acid variant BAG3-T285D/S289D (Figure 3E), and RAB7A, RAB1A, RAB2A/B, and RAB10 showed increased binding to BAG3-T285A compared to T285D (Figure S3F). The data point to a force-induced, dephosphorylation-dependent interaction of BAG3 with a subset of small GTPases. RAB GTPases regulate intracellular membrane traffic and compartmentalization in eukaryotic cells.[31] Strikingly, all BAG3-associated RABs, except RAB11B, were previously linked to autophagy.[32–40] Their regulated association with BAG3 under mechanical stress may thus facilitate membrane fusion events during CASA.

RAB7A and RAB11B are essential for CASA

To explore the relevance of BAG3-associated RABs for skeletal muscle homeostasis, RABs were depleted by RNA interference in differentiating murine skeletal muscle cells (Figure 4A). In

Please cite this article in press as: Ottensmeyer et al., Force-induced dephosphorylation activates the cochaperone BAG3 to coordinate protein homeostasis and membrane traffic, Current Biology (2024), https://doi.org/10.1016/j.cub.2024.07.088

CellPress
OPEN ACCESS

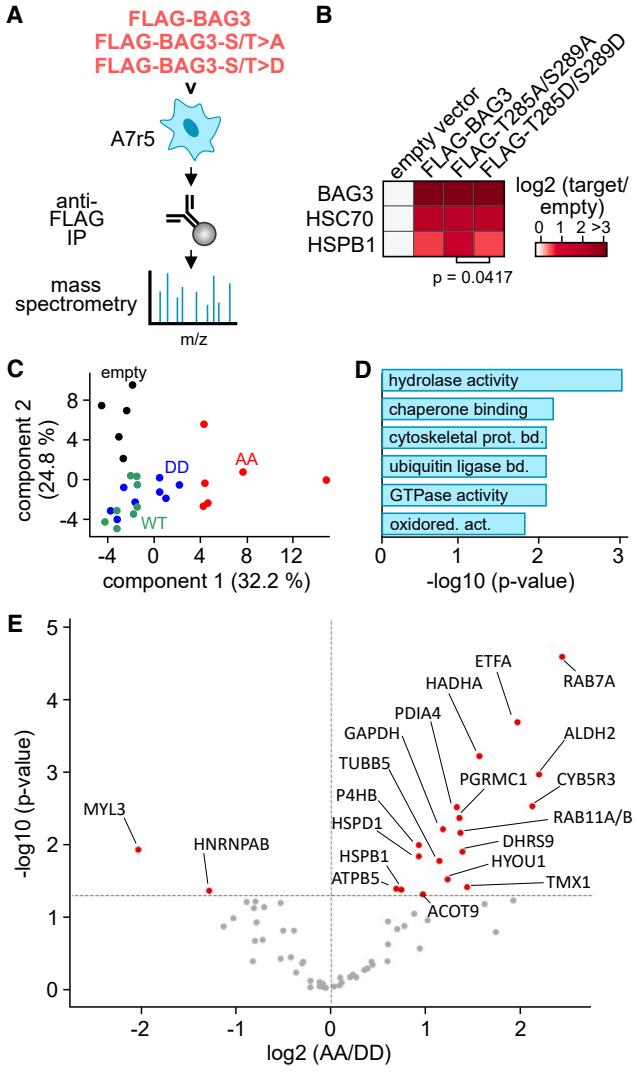

Figure 3. BAG3 interacts with RAB GTPases in a dephosphorylation-dependent manner

(A) Phosphosite mutant variants of BAG3 were transiently expressed in A7r5 cells as FLAG-epitope tagged proteins followed by anti-FLAG immunoprecipitation and mass spectrometry.

(B) HSC70 was detected in complexes of wild-type BAG3, and BAG3-T285A/S289A and BAG3-T285D/S289D mutant variants by interaction proteomics. HSPB1 was significantly more abundant (LIMMA-moderated t test p value < 0.05) in pull-downs with the dephosphorylation-mimicking BAG3-T285A/S289A. Heatmap shows protein abundance as $\log_2$-transformed mean intensity compared to mean background intensity (FLAG-BAG3-construct/empty). See Data S1A for more information.

(C) Principal-component analysis based on label-free quantification (LFQ) intensities of 42 proteins identified as differentially abundant (ANOVA p value < 0.05 with Tukey's post hoc test FDR < 0.05). Empty, empty vector transfected controls (black); WT, wild-type BAG3 (green); DD, BAG3-T285D/S289D (blue); AA, BAG3-T285A/S289A (red). See Data S1B for more information.

(D) Gene Ontology (GO) terms enriched among proteins identified as BAG3 interactors. GO terms were selected from significantly enriched categories (FDR-corrected p value < 0.05). For GO-term identifier numbers, see Data S1C.

(E) Volcano plot visualizing the $\log_2$ transformed ratio of mean protein abundance in pull-downs with BAG3-T285A/S289A compared to BAG3-T285D/S289D ($\log_2$ (AA/DD)), plotted against $-\log_{10}$ (LIMMA-moderated t test p value AA/DD) as a measure of significance. See Data S1D for more information.

For all panels: empty vector, n = 5; FLAG-BAG3, n = 8; FLAG-T285D/S289D, n = 8; FLAG-T285A/S289A, n = 6.

See also Figure S3 and Table S1 and Data S2.

this approach, we used C2 myoblasts, the parental cell line from which the C2C12 cell line was derived.[41] Following differentiation to myotubes, cells were treated with bafilomycin A1 (BafA1), which prevents the acidification of lysosomes and thereby blocks late stages of autophagy, resulting in the accumulation of autophagy clients. Besides core autophagy factors such as SQSTM1 and lipidated LC3B (LC3B-II), BAG3 and SYNPO2 were analyzed as CASA-specific components (Figure 4B). We concentrated on RAB2A and RAB11A/B, which were detected in complexes with BAG3-T285A and BAG3-T285A/S289A, respectively, and on RAB7A that was significantly enriched in both complexes (Figures 3E and S3F). RNA interference reduced RAB2A levels in differentiated myotubes to ~30% (Figures S4A and S4B). RAB2A depletion was accompanied by an increase in the steady-state level of LC3B-II, whereas BAG3, SYNPO2, and SQSTM1 levels remained unaffected (Figure S4B). BafA1 treatment of differentiated myotubes revealed autophagic degradation of BAG3, SYNPO2, SQSTM1, and LC3B-II, which was not significantly altered upon RAB2A depletion (Figure S4C). Regarding the RAB11 isoforms A and B, we initially focused on RAB11A because of its role in AP assembly.[39] Following small interfering RNA (siRNA) treatment, RAB11A was no longer detectable in myotubes (Figure S4D). Whereas SYNPO2, SQSTM1, and LC3B-II steady-state levels were not altered upon RAB11A depletion, BAG3 levels were ~1.5-fold increased (Figures S4D and S4E). Impairment of membrane traffic in the absence of RAB11A might be compensated by elevated BAG3 expression. Indeed, autophagic degradation rates were not significantly different between control and RAB11A-depleted cells (Figure S4F). Taken together, depletion of RAB2A and RAB11A, respectively, leads to an adaptation of the autophagy network in differentiated myotubes, but both GTPases are dispensable for autophagic flux and CASA activity.

A different picture emerged for RAB11B. Although, RAB11B has not been linked to autophagy in previous studies, its depletion to about 45% of the control level completely abrogated the autophagic degradation of BAG3 and SYNPO2 (Figures 4B and 4D). In contrast, SQSTM1 and LC3B-II turnover was not affected by RAB11B depletion. RAB11B is apparently not generally required for autophagic flux in skeletal muscle cells but exerts specific and essential functions during CASA.

An essential role in CASA was also revealed for RAB7A, which was the most robust interactor of BAG3 dephosphorylation mimicry variants (Figures 3E and S3F). The established siRNA strategy allowed us to deplete RAB7A in C2 myotubes to about 50% of the control level (Figures 4E and 4F). RAB7A depletion led to an increase of the steady-state levels of BAG3, SQSTM1, and LC3B-II (Figure 4F). Furthermore, autophagic degradation of all analyzed components was significantly reduced to about half of the degradation rate in control cells (Figure 4G). The data show that RAB7A is a core autophagy factor in skeletal muscle cells, involved in CASA and other SQSTM1 and LC3B-dependent autophagy pathways.

Please cite this article in press as: Ottensmeyer et al., Force-induced dephosphorylation activates the cochaperone BAG3 to coordinate protein homeostasis and membrane traffic, Current Biology (2024), https://doi.org/10.1016/j.cub.2024.07.088

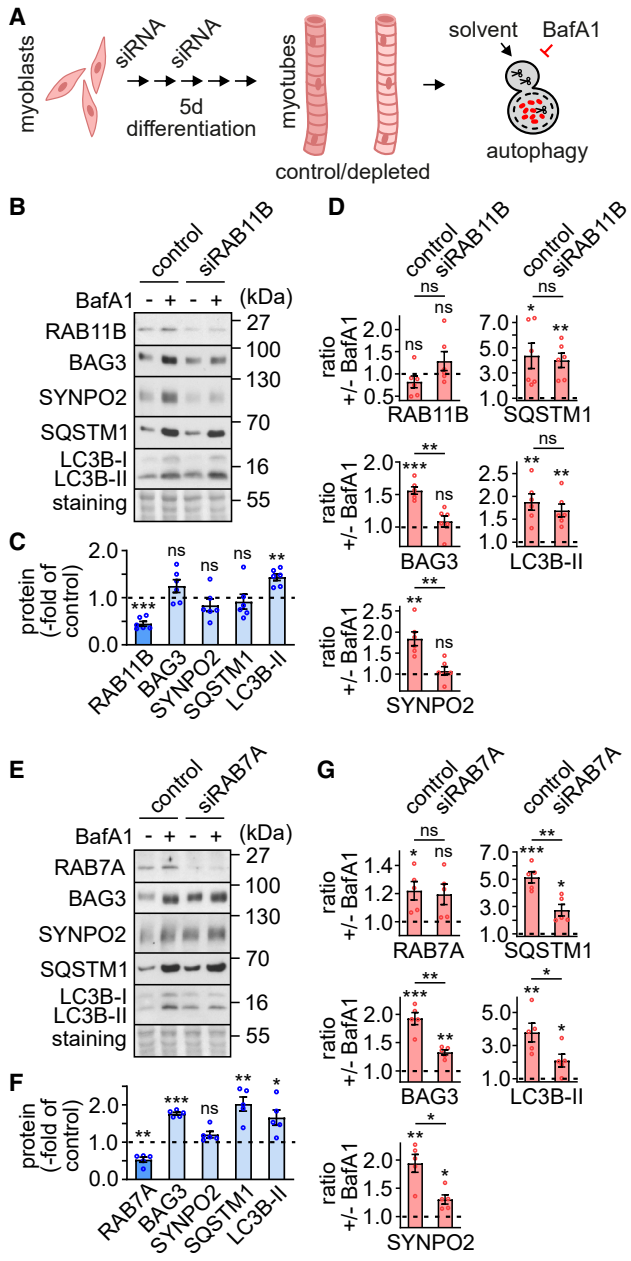

Figure 4. RAB11B and RAB7A are essential for CASA in differentiated mouse myotubes

(A) C2 mouse myoblasts were differentiated to myotubes for 5 days. At days 0 and 2 siRNA transfections were performed. Obtained myotubes were treated with the solvent DMSO or the autophagy inhibitor bafilomycin A1 (BafA1) to determine autophagic activity.

(B) Differentiated myotubes, transfected with control siRNA or RAB11B-targeting siRNA (siRAB11B), were incubated with solvent (−) or BafA1 (+) for 5 h. Myotube lysates were analyzed with specific antibodies against the indicated proteins.

(C) RAB11B depletion leads to an increase in the steady-state level of LC3B-II. Data obtained under (B) were quantified. Protein levels observed in solvent-treated and control siRNA-transfected cells were set to 1 and were compared to levels in solvent-treated RAB11B-depleted cells. The dashed line indicates the control value. Data are shown as mean values ± SEM, $n = 6$.

(D) RAB11B depletion specifically attenuates CASA. Data obtained under (B) were quantified. The ratio of protein levels with and without BafA1 treatment (ratio ± BafA1) was determined. The dashed line indicates a ratio of 1 with no changes upon BafA1 treatment. Data are shown as mean values ± SEM, $n = 6$.

(E) Differentiated myotubes, transfected with control siRNA or RAB7A-targeting siRNA (siRAB7A), were incubated with solvent (−) or BafA1 (+) for 5 h. Myotube lysates were analyzed with specific antibodies against the indicated proteins.

(F) RAB7A depletion leads to an increase in the steady-state levels of BAG3, SQSTM1, and LC3B-II. Data obtained under (E) were quantified. Protein levels observed in solvent-treated and control siRNA-transfected cells were set to 1 and were compared to levels in solvent-treated RAB7A-depleted cells. The dashed line indicates the control value. Data are shown as mean values ± SEM, $n = 5$.

(G) RAB7A depletion attenuates autophagic flux. Data obtained under (E) were quantified. The ratio of protein levels with and without BafA1 treatment (ratio ± BafA1) was determined. The dashed line indicates a ratio of 1 with no changes upon BafA1 treatment. Data are shown as mean values ± SEM, $n = 5$.

Statistical analysis was carried out using two-tailed unpaired t test with Welch's correction: $^{*}p < 0.05$, $^{**}p < 0.01$, $^{***}p < 0.001$; ns, non-significant. Asterisks above column bars indicate significance compared with control. Asterisks above columns-connecting lines indicate significance between the compared samples.

See also Figure S4.

RAB7A exerts early and late functions during CASA and directly interacts with BAG3

Previous work has highlighted a role of RAB7A in AP maturation and AP-lysosome fusion.[32] Engulfment of BAG3 by phagophore membranes during AP formation apparently reduces the availability of the cochaperone for binding to RAB7A at these late stages of autophagy. We therefore investigated whether RAB7A also acts early during AP formation in cells with active CASA. A7r5 rat smooth muscle cells were cultivated on fibronectin to induce CASA and were transfected with a plasmid for expression of an LC3B-traffic-light reporter protein (mCherry-EGFP-LC3B). In APs, the reporter protein emits green and red fluorescence, causing a yellow appearance in merged images, whereas quenching of the EGFP portion in acidic ALs results only in red fluorescence (Figure 5A). Thus, the reporter protein allows to simultaneously quantify APs and ALs in transfected cells (Figure 5B). To verify a role of RAB7A in AP and AL formation, dominant-negative RAB7A-T22N was co-expressed with mCherry-EGFP-LC3B. The mutation reduces the affinity for guanosine triphosphate (GTP) and impairs nucleotide exchange on RAB7A.[42] Co-expression of RAB7A-T22N increased the ratio between APs and ALs (AP/AL) (Figure 5C, red columns). Consistent with the function of RAB7A in AP-lysosome fusion, the maturation of APs is apparently attenuated in the presence of mutant RAB7A. Strikingly, however, impaired AP-lysosome fusion did not result in an accumulation of APs in A7r5 cells (Figure 5C, yellow columns). This is in marked contrast to previous findings for starvation-induced autophagy, where RAB7A-T22N expression caused a strong increase in AP number due to impaired late stages of autophagy.[43] The lack of AP accumulation observed here in CASA-executing cells suggests that RAB7A does not only stimulate AP-lysosome fusion but also contributes to the initial formation of APs during CASA (Figure 5D).

In vitro binding experiments with purified proteins were performed to test for a direct interaction between BAG3 and RAB7A. The dephosphorylation-mimicking BAG3-T285A/S289A was incubated with T7-tagged RAB7A followed by anti-T7 immunoprecipitation (Figure 5E). As effector protein binding to RAB7A

Please cite this article in press as: Ottensmeyer et al., Force-induced dephosphorylation activates the cochaperone BAG3 to coordinate protein homeostasis and membrane traffic, Current Biology (2024), https://doi.org/10.1016/j.cub.2024.07.088

CellPress
OPEN ACCESS

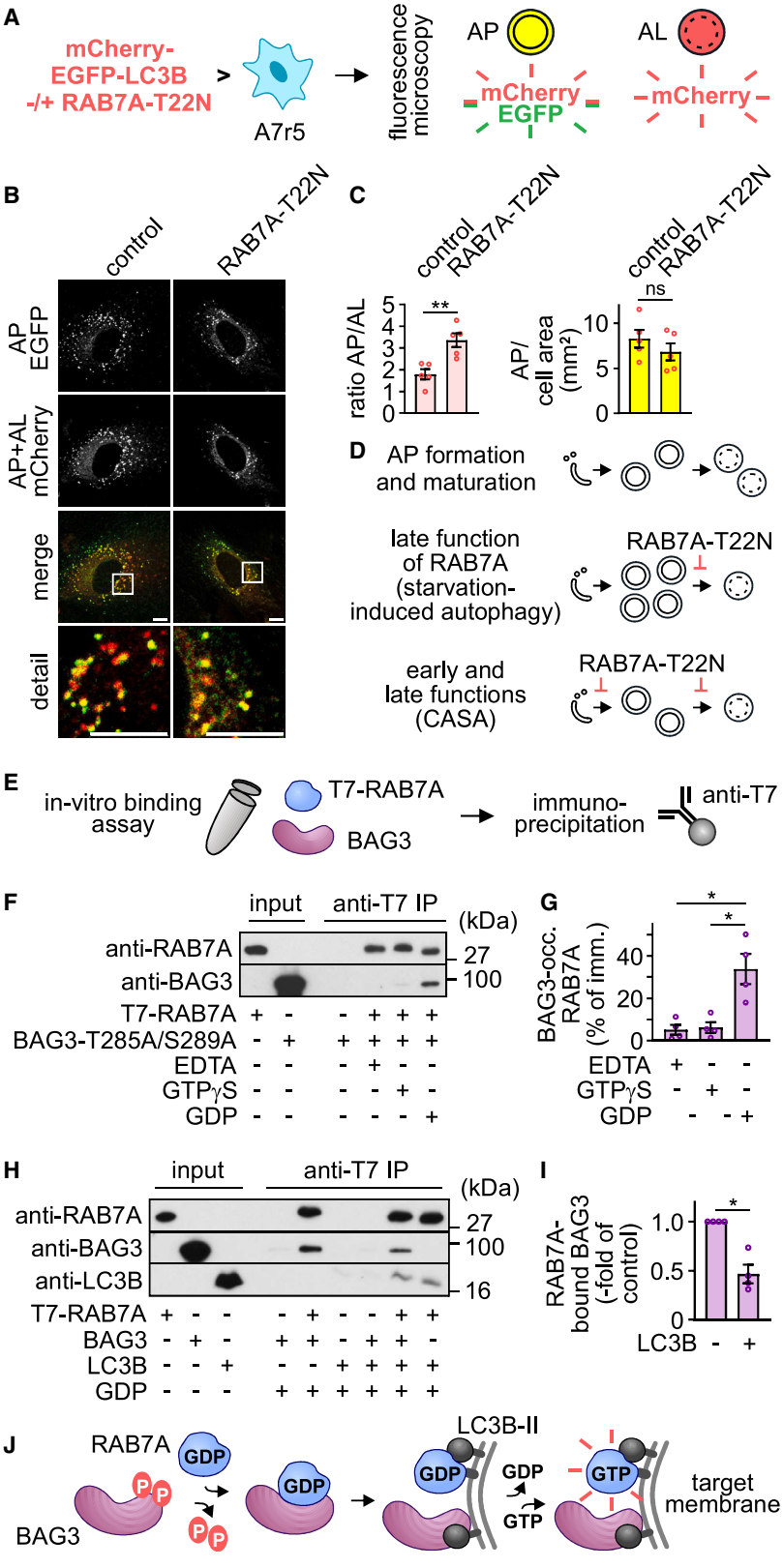

Figure 5. RAB7A acts in autophagosome formation and autophagosome-lysosome fusion in smooth muscle cells and is recognized by dephosphorylated BAG3 when in the GDP-bound state

(A) An LC3B traffic-light construct (mCherry-EGFP-LC3B) was expressed in A7r5 smooth muscle cells. Expression of the reporter protein allows to distinguish between autophagosomes (AP, yellow fluorescence) and autolysosomes (AL, red fluorescence).

(B) A7r5 cells were transfected with mCherry-EGFP-LC3B together with an empty plasmid (control) or with one that encodes for the dominant-negative mutant variant RAB7A-T22N. Cells were grown on fibronectin-coated plates to induce CASA activity. 48 h after transfection cells were fixed and subjected to confocal microscopy. Scale bars represent 10 μm.

(C) The number of autophagosomes per cell area (AP/cell area [mm^2]) was determined in control and RAB7A-T22N expressing cells, and the AP/AL ratio was calculated. For quantification, at least 20 cells of each condition were analyzed in each of 5 independent experiments. Data are shown as mean values ± SEM, $n = 5$.

(D) Schematic presentation of autophagy pathway disruption in the presence of RAB7A-T22N.

(E) Purified T7-RAB7A and BAG3 variants were used in *in vitro* binding experiments followed by immunoprecipitation with an anti-T7 antibody.

(F) Incubation of equimolar concentrations of purified proteins (1 μM) was performed in the presence of EDTA, GPTγS, or GDP as indicated. Isolated complexes were analyzed by western blotting with specific antibodies against RAB7A and BAG3. Input corresponds to 10% of the total sample, and IP sample represents 20% of the eluate.

(G) Data obtained under (F) were quantified. Levels of co-immunoprecipitated BAG3 were determined and normalized for the levels of immunoprecipitated RAB7A. Data are given as BAG3-occupied RAB7A in percent of total immunoprecipitated RAB7A (BAG3-occ.RAB7 [% of imm.]) and are shown as mean values ± SEM, $n = 4$.

(H) Equimolar concentrations (1 μM) of purified RAB7A, BAG3, and LC3B were incubated in the presence of GDP as indicated, followed by isolation of RAB7A and associated proteins by immunoprecipitation with an anti-T7 antibody. Isolated complexes were analyzed by western blotting with specific antibodies against RAB7A and BAG3. Input corresponds to 5% of the total sample, and IP sample represents 20% of the eluate.

(I) Data obtained under (H) were quantified. BAG3 levels detected in association with RAB7A in the absence of LC3B were set to 1, and the fold change in the presence of LC3B was calculated. Data are shown as mean values ± SEM, $n = 4$.

(J) Schematic presentation of the regulated interaction between BAG3 and RAB7A during autophagosome formation.

Statistical analysis was carried out using two-tailed unpaired t test with Welch's correction: $^*p < 0.05$, $^{**}p < 0.01$; ns, non-significant.

See also Figure S5.

Please cite this article in press as: Ottensmeyer et al., Force-induced dephosphorylation activates the cochaperone BAG3 to coordinate protein homeostasis and membrane traffic, Current Biology (2024), https://doi.org/10.1016/j.cub.2024.07.088

is dependent on the nucleotide state of the GTPase,[44] proteins were incubated in the presence of EDTA to induce a nucleotide-free state or with non-hydrolysable GTP-γ-S or guanosine diphosphate (GDP). Notably, an association of BAG3-T285A/S289A with GDP-loaded RAB7A was observed (Figures 5F and 5G). The GDP-bound state represents the inactive form of RAB7A, which is largely localized in the cytoplasm.[44] Also, recombinantly expressed and purified wild-type BAG3 was used in binding assays. The bacterially expressed protein does not display the phosphorylation pattern characteristic for inactivated BAG3 in mammalian cells, as is evident from the lack of S136 phosphorylation (Figure S5A). It may therefore behave like activated BAG3. Indeed, the recombinant wild-type protein also interacted with GDP-bound RAB7A (Figure 5H). Next, a possible impact of the autophagic membrane marker LC3B on the interaction between BAG3 and RAB7A was investigated because BAG3 directly binds to LC3B[45] and RAB7A is part of the LC3B interactome.[46] When purified LC3B was included in *in vitro* binding assays, a direct interaction between RAB7A and LC3B was detected (Figure 5H). Importantly, the presence of LC3B significantly reduced binding of BAG3 to RAB7A (Figure 5H). Taken together, our findings suggest a pathway on which force-induced dephosphorylation of BAG3 triggers an interaction of the cochaperone with inactive RAB7A-GDP throughout the cytoplasm followed by sorting to sites of AP formation (Figure 5J). LC3B-facilitated docking onto phagophore membranes then leads to a dissociation and subsequent activation of RAB7A to promote phagophore fusion.

Induction of mitophagy triggers BAG3 dephosphorylation in skeletal muscle cells

RAB7A also exerts early functions during the engulfment of damaged mitochondria by autophagic membranes.[33,47] Intriguingly, BAG3 is recruited to damaged mitochondria and promotes mitophagy.[48] We therefore investigated whether induction of mitophagy affects BAG3 phosphorylation. Toward this end, C2 myotubes were treated with carbonyl cyanide 3-chlorophenylhydrazone (CCCP) and valinomycin. Both compounds lead to a disruption of the mitochondrial membrane potential and trigger mitophagy.[49,50] Mitophagy induction was verified by detection of ubiquitin phosphorylated on serine-65 (ubiquitin-pS65) (Figure S5B), which is generated upon activation of the mitophagy-stimulating kinase PINK1.[51] Notably, mitophagy induction led to a significant increase in BAG3 expression in differentiated skeletal muscle cells and triggered an almost complete dephosphorylation of BAG3 (Figures S5B and S5C). Dephosphorylation-dependent activation of BAG3 may thus not only stimulate AP formation during CASA but also facilitate mitophagy.

Overactivation of CASA in RAB7A-L129F patient cells may contribute to neuropathy

The identification of RAB7A as an essential CASA component has implications beyond muscle homeostasis. Mutations in RAB7A as well as in HSPB1, HSPB8, and BAG3 cause Charcot-Marie-Tooth type 2 (CMT2) neuropathy, which is characterized by a loss of peripheral neurons.[42,52–58] The prevalent hypothesis to explain RAB7A-related CMT2 pathology is that mutant alleles alter endosome-lysosome trafficking and thereby impair neurotrophic signaling.[59] To investigate whether dysregulation of CASA could contribute to the observed pathology, degradation assays were performed with lymphoid cells from a CMT2 patient expressing RAB7A-L129F.[60] This amino acid substitution makes cycling between GDP and GTP-bound states largely independent of a cognate guanine nucleotide exchange factor (GEF) and a GTPase-activating protein (GAP), leading to increased levels of activated RAB7A-L129F (Figure 6A).[61] The cellular concentration of RAB7A-L129F in patient cells was reduced to about 50% of the concentration of the wild-type protein in healthy control cells (Figures 6B and 6C). Moreover, a significant accumulation of RAB7A-L129F was observed in patient cells after treatment with the autophagy inhibitor BafA1 (Figures 6B and 6D). Excessive activation of RAB7A-L129F apparently results in increased autophagic degradation of the GTPase and, consequently, lowers its cellular concentration. Strikingly, RAB7A reduction in patient cells was accompanied by a reduction of BAG3 levels (Figures 6B and 6C). In addition, autophagic turnover of BAG3 and SYNPO2 was significantly increased in patient cells (Figures 6B and 6D). The CMT2-causing L129F mutation in RAB7A apparently causes an overactivation of CASA in patient cells.

DISCUSSION

Here, we uncover molecular details of the force-dependent regulation of BAG3. We demonstrate that BAG3 is dephosphorylated in response to internally generated and externally applied mechanical forces in diverse mammalian tissues and cell types. Dephosphorylation of BAG3 triggers an association with sHSPs and activates CASA through binding to autophagy-stimulating RAB GTPases (Figure 6E).

A phospho-switch for a regulated interaction with sHSPs is formed by residues T285 and S289 of BAG3. The residues are distantly located from the two isoleucine-proline-valine (IPV) motifs of BAG3 (amino acid [aa] 96–98 and 208–210) that mediate the interaction with sHSPs (Figure 1A).[62] The phospho-switch apparently regulates the accessibility of the IPV motifs through induced conformational changes of BAG3. sHSPs form oligomeric assemblies with a unique capacity to stabilize misfolded proteins.[63] Upon proteasome impairment, the sHSP HSPB8 acts upstream of BAG3 to sequester ubiquitylated proteins in microaggregates that are subsequently concentrated through BAG3-dependent transport along microtubules for final autophagic degradation.[64] The phospho-switch in BAG3 may allow to uncouple the chaperone and surveillance function of HSPB8 from a degradative function that is exerted in conjunction with BAG3. Remarkably, regulated uncoupling of BAG3 and HSPB8 is important for the biogenesis of stress granules (SGs), which are membrane-less assemblies for the storage of mRNA under stress conditions.[65] In response to oxidative stress, for example, HSPB8 dissociates from BAG3 and is incorporated into SGs to stabilize SG components. When the stress subsides, the interaction between BAG3 and HSPB8 is re-established, which is necessary for SG disassembly.[65] Phosphorylation and dephosphorylation on T285 and S289 of BAG3 could provide the molecular basis for a dynamic and regulated interplay between the cochaperone and the sHSP under these conditions.

HSPB8 closely cooperates with BAG3 during CASA and stimulates the association of BAG3 with the autophagic ubiquitin

Please cite this article in press as: Ottensmeyer et al., Force-induced dephosphorylation activates the cochaperone BAG3 to coordinate protein homeostasis and membrane traffic, Current Biology (2024), https://doi.org/10.1016/j.cub.2024.07.088

CellPress
OPEN ACCESS

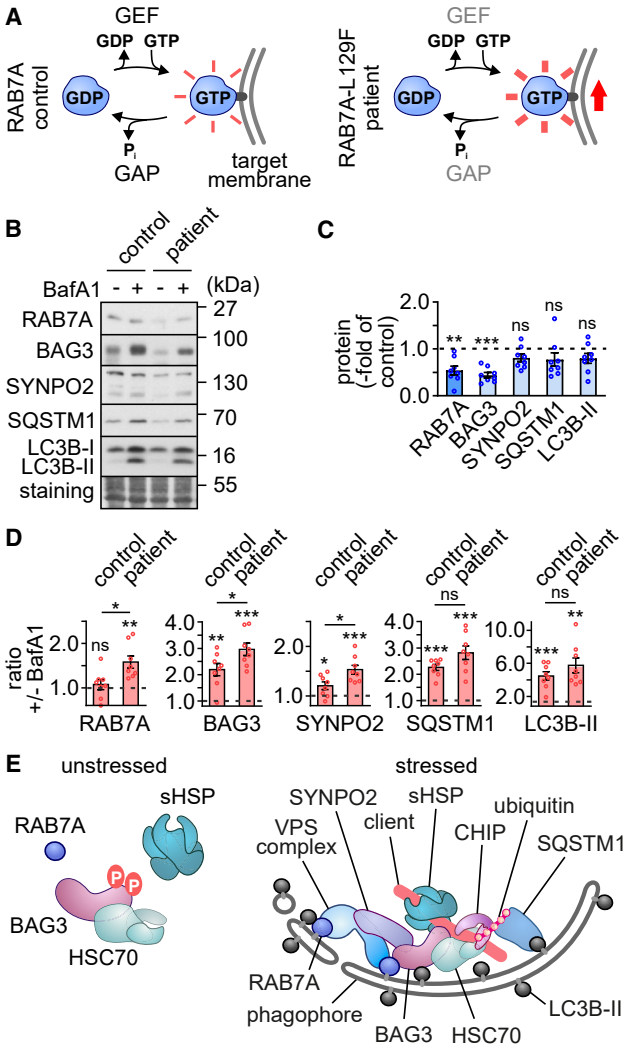

Figure 6. CMT2-causing RAB7A-L129F induces an overactivation of CASA in patient cells

(A) Schematic presentation of the altered GTPase cycle of RAB7A-L129F as determined by McCray et al.[61] RAB7A activity is controlled by a guanine nucleotide exchange factor (GEF) and a GTPase-activating protein (GAP).

(B) Lymphoid cells of a control subject and CMT2 patient were treated with solvent (–) or BafA1 (+) for 7 h. Lysates were probed with specific antibodies against the indicated proteins. Multiple isoforms of SYNPO2 are detectable in this cell type.

(C) Data obtained under (B) were quantified. Protein levels observed in solvent-treated control cells were set to 1 and were compared to levels in solvent-treated patient cells to determine changes in the steady-state levels. The dashed line indicates the control value. Data are shown as mean values ± SEM, $n = 4$ with two biological replicates performed in each independent experiment.

(D) Data obtained under (B) were quantified. The ratio of protein levels with and without BafA1 treatment (ratio ± BafA1) was determined. The dashed line indicates a ratio of 1 with no changes upon BafA1 treatment. Data are shown as mean values ± SEM, $n = 4$ with two biological replicates performed in each independent experiment.

(E) Schematic presentation of the stress-dependent regulation of BAG3.

Statistical analysis was carried out using two-tailed unpaired t test with Welch's correction: $^*p < 0.05$; ns, non-significant.

adaptor SQSTM1.[64] In addition to HSPB8, BAG3 also binds to HSPB1, HSPB5, and HSPB6.[29] It has remained unclear, however, whether these sHSPs contribute to BAG3-mediated autophagy. Strikingly, we observed that HSPB8 is not expressed in A7r5 smooth muscle cells (Figure S3A), although high CASA activity is detected in this cell type when grown on fibronectin (Figure 2E).[9] Instead of HSPB8, HSPB1 was identified as a dephosphorylation-dependent interactor of BAG3 in A7r5 cells (Figures 3B and 3E). Knock down of HSPB1 or the expression of disease-causing mutant variants attenuates autophagic degradation in diverse cell types.[52] Moreover, HSPB1 binds directly to SQSTM1 and triggers the formation of SQSTM1 scaffolds necessary for phagophore formation.[52] In this way, HSPB1 could facilitate CASA upon association with BAG3 and functionally replace HSPB8. In fact, depletion of HSPB1 abrogated CASA in smooth muscle cells (Figures S3B and S3C), demonstrating a cooperation between BAG3 and HSPB1 in autophagic protein degradation.

Phosphorylation mimicry on residues S136, T285, and T285/S289, respectively, results in mutant variants of BAG3, which inhibit CASA activity in a dominant-negative manner (Figure 2E). S136 is the terminal residue of the first of two 14-3-3 binding sites within BAG3 (Figure 1A). Binding of BAG3 to 14-3-3 proteins increases the association with dynein motor proteins and promotes the microtubule-dependent transport of misfolded protein cargo into perinuclear aggresomes.[22] Remarkably, aggresome targeting was enhanced by phosphorylation of S136,[22] whereas CASA activity, monitored by SYNPO2 degradation, was attenuated (Figure 2E). This implies a highly dynamic, S136-regulated process in which phosphorylation-dependent sequestration of cargo is followed by dephosphorylation-dependent AP formation and degradation. Release of BAG3 from transport complexes might be necessary in this scenario for cargo enclosure by phagophore membranes. Yet, differential proteomics did not reveal an increased association of the dephosphorylation-mimicking S136A variant with proteostasis or autophagy factors (Table S1). It appears that rather transient low-affinity interactions are regulated through S136 phosphorylation and dephosphorylation.

In contrast, the phosphorylation status of residues T285 and T285/S289 controls the association of BAG3 with autophagy-stimulating RAB GTPases (Figures 3E and S3F). RAB1A, RAB2A/B, RAB7A, RAB10, and RAB11A/B all showed preferential binding to force-activated, dephosphorylated variants of BAG3. RAB1 and RAB2 isoforms link the endoplasmic reticulum and the Golgi apparatus to the autophagy network, as they facilitate membrane trafficking at these compartments and, in addition, affect the localization of autophagy-inducing kinases to promote autophagy initiation.[35–37,66] RAB10 mediates membrane trafficking between the Golgi and the plasma membrane and stimulates the formation of recycling endosomes, but also associates with nascent phagophores to trigger cargo engulfment during lipophagy and mitophagy.[34,38] Finally, RAB11A regulates the trafficking of recycling endosomes and directs such endosomes to sites of AP formation in the context of mitophagy and starvation-induced autophagy.[39,67] The observed dephosphorylation-dependent association of BAG3 with the aforementioned RABs may thus allow to recruit membrane vesicles of different origins for AP formation during CASA. The participating

Please cite this article in press as: Ottensmeyer et al., Force-induced dephosphorylation activates the cochaperone BAG3 to coordinate protein homeostasis and membrane traffic, Current Biology (2024), https://doi.org/10.1016/j.cub.2024.07.088

RABs likely exert overlapping functions. Indeed, depletion of either RAB2A or RAB11A in mouse myotubes did not attenuate CASA activity (Figure S4). Directing membrane material from multiple sources into the CASA pathway may ensure robust and efficient disposal of abundant cytoskeleton proteins following their damage under mechanical stress.

In contrast to RAB11A, depletion of RAB11B abrogated CASA in differentiated skeletal muscle cells (Figures 4B and 4D). Even though the two isoforms share a high degree of sequence homology and have both been linked to endosomal recycling pathways, RAB11A and RAB11B reside on distinct vesicle compartments and exert specific functions in the recycling of different plasma membrane proteins.[68–70] Furthermore, it is unclear whether RAB11B facilitates phagophore formation as does RAB11A. Although the intersection between RAB11B-mediated membrane traffic and the CASA pathway remains to be defined, it is striking that RAB11B depletion interfered with CASA but did not generally block SQSTM1- and LC3B-mediated autophagy in mouse myotubes (Figures 4B and 4D). The dephosphorylation-induced association of BAG3 with RAB11B seems to promote a specific recruitment of RAB11B decorated vesicles onto the CASA pathway. Notably, RAB11B expression is induced by mechanical stress, and RAB11B affects mechanotransduction by regulating integrin receptor recycling.[71,72] The observed essential role of RAB11B in CASA thus adds a new facet to the homeostatic function of the GTPase in mechanically challenged cells and tissues.

While RAB11B exerted CASA-specific functions, RAB7A emerged here as a general autophagy factor, whose depletion attenuated the degradation of CASA components as well as of core autophagy proteins (Figures 4E and 4G). RAB7A acts in endosome-lysosome trafficking and facilitates late stages of autophagy, i.e., AP -lysosome fusion.[32,43,73–75] Consistent with such a function, we observed that the AP to AL ratio was increased in CASA-executing A7r5 cells that express dominant-negative RAB7A-T22N (Figures 5B and 5C). A role of BAG3 in endosome-lysosome trafficking and in late stages of AP maturation has been revealed in neuronal cells,[6,76] and might involve cooperation with RAB7A. In fact, BAG3 regulates the GTPase RAB35 during endosome trafficking in neurons, which highlights the importance of the interplay of BAG3 with RAB proteins.[76] However, BAG3 also exerts a prominent role in autophagy initiation and cooperates with SYNPO2 to mediate phagophore fusion during cargo engulfment in skeletal and smooth muscle cells (Figure 6E).[9] Multiple lines of evidence suggest that RAB7A acts at early stages of CASA. First, an accumulation of APs was not observed in A7r5 cells upon expression of dominant-negative RAB7A-T22N (Figures 5B and 5C). This is in marked contrast to findings for starvation-induced autophagy in Chinese hamster ovary (CHO) cells, where RAB7A-T22N expression caused a strong increase in AP number.[43] It suggests that the mutant RAB interferes with AP closure in CASA-executing cells. Moreover, RAB7A was the only RAB, which significantly accumulated upon autophagy inhibition in myotubes (Figure 4G). A fraction of RAB7A apparently becomes enclosed by AP membranes and is then co-degraded. Again, this points to a role of RAB7A in AP formation during CASA. Of note, RAB7A was recently also identified as autophagy cargo in basal autophagy and shown to facilitate the engulfment of damaged mitochondria by phagophores during mitophagy.[33,38,46,47,77] Thus, RAB7A stimulates early membrane fusion events on diverse autophagy pathways, including CASA.

During mitophagy, RAB7A associates with damaged organelles and induces their autophagic engulfment through recruitment of ATG9A-positive lipid vesicles for phagophore expansion.[77] Mitochondrial association of RAB7A is dependent on the MON1/CCZ1 complex, which acts as a GDP/GTP exchange factor of RAB7A.[78,79] The complex binds to cytosolic GDP-bound RAB7A and directs the GTPase to damaged mitochondria.[77] In a striking analogy, we observed that BAG3 also binds to GDP-bound RAB7A (Figures 5F–5I). We, therefore, propose a model for CASA initiation under stress in which dephosphorylation-dependent binding of BAG3 to cytosolic RAB7A triggers recruitment to sites of AP formation, where RAB7A would facilitate phagophore expansion (Figures 5J and 6E). Importantly, association with LC3B weakens the interaction between RAB7A and BAG3 (Figures 5H and 5I). Binding of LC3B to BAG3 as well as to RAB7A may promote complex dissociation, as an LC3B-interacting region (LIR) was recently identified in BAG3[45] and a direct interaction between LC3B and RAB7A was revealed here (Figure 5H). Upon release of RAB7A from BAG3 at the phagophore, the GTPase would become available for activation and could then associate with a membrane tethering complex to mediate phagophore fusion. In fact, a VPS16 and VPS18-containing membrane tethering complex, which resembles the RAB7A-binding HOPS complex on late endosomes and lysosomes,[80] is contacted by SYNPO2 during BAG3-mediated autophagy (Figure 6E).[9]

As energy-generating organelles, mitochondria are required for maintaining healthy muscle, and exercise improves mitochondrial activity by stimulating the synthesis of new organelles and the mitophagic clearance of damaged ones.[81–83] Remarkably, altered mitochondrial morphology has been observed in hearts of BAG3 mutant mice.[16,84] Furthermore, BAG3 associates with damaged mitochondria and promotes mitophagy in rat cardiomyocytes.[48] Exercise-induced binding of BAG3 to RAB7A may explain this mitophagy-stimulating activity of BAG3, as it would increase the concentration of RAB7A on the mitochondrial surface to facilitate mitophagosome formation. An involvement of BAG3 in the initiation of CASA and mitophagy could enable the cochaperone to coordinate both degradation pathways during muscle maintenance. In agreement with a crosstalk of CASA and mitophagy, pharmacological induction of mitophagy in skeletal muscle cells triggered BAG3 expression and dephosphorylation (Figures S5B and S5C).

The proteostasis function of BAG3 is not restricted to muscle cells. BAG3 is also essential for protein homeostasis in neurons, where it degrades aggregation-prone proteins such as the microtubule-binding protein tau, which accumulates in Alzheimer's disease.[5,6] Intriguingly, mutations in RAB7A, BAG3, HSPB8, and HSPB1 all can cause Charcot-Marie-Tooth type 2 (CMT2) neuropathy characterized by a length-dependent degeneration of peripheral neurons.[52,53,56,58,60,85,86] RAB7A-associated pathology was so far mainly attributed to altered endosome-lysosome trafficking.[60,85,86] However, our identification of RAB7A as an essential CASA component suggests that dysregulation of the autophagy pathway could contribute to disease progression upon expression of RAB7A mutant variants. Indeed, the disease variant RAB7A-L129F, which displays elevated activation,[61] stimulated CASA in CMT2 patient cells (Figures 6B and

6D). Overactivation of the CASA pathway may directly impair tau and microtubule homeostasis and thereby adversely affect axon stability, neurotrophic signaling, and neuronal survival.

Pharmacological modulation of BAG3-mediated proteostasis holds the promise to treat some of the most prevalent diseases of our time, including heart failure and neurodegeneration. Our characterization of phospho-switches in BAG3 reveals a regulatory mechanism in which BAG3-inhibiting kinases and BAG3-activating phosphatases control CASA complex formation and CASA initiation. Although the involved kinases and phosphatases remain to be identified, elucidating BAG3-regulating signaling networks could help to find druggable target proteins for therapeutic intervention in BAG3-related pathologies.

STAR★METHODS

Detailed methods are provided in the online version of this paper and include the following:

- KEY RESOURCES TABLE
- RESOURCE AVAILABILITY
  - Lead contact
  - Materials availability
  - Data and code availability
- EXPERIMENTAL MODEL AND STUDY PARTICIPANT DETAILS
  - Human study
  - Cell lines
- METHOD DETAILS
  - Human study design
  - Resistance exercise (RE)
  - Standardized mechanical overload (SMO)
  - Skeletal muscle biopsies
  - Generation and validation of the anti-BAG3-pS136 antibody
  - Electrical pulse stimulation
  - Unidirectional cyclic stretch
  - Generation and characterization of phosphosite mutant variants of BAG3
  - Proteome preparation and mass spectrometry
  - Proteome data analysis
  - Monitoring autophagic degradation following RNA interference
  - Autophagosome formation and maturation assay
  - In-vitro binding assays
  - Analysing BAG3 dephosphorylation upon mitophagy induction
  - Cultivation and analysis of CMT2 patient cells
- QUANTIFICATION AND STATISTICAL ANALYSIS

SUPPLEMENTAL INFORMATION

Supplemental information can be found online at https://doi.org/10.1016/j.cub.2024.07.088.

ACKNOWLEDGMENTS

We thank Karen Himmelberg (Bonn, Germany) and Vicky De Winter (Antwerp, Belgium) for expert technical assistance. Maja Köhn (Freiburg, Germany) is acknowledged for stimulating discussions during the preparation of the manuscript, and Wolfgang Voos (Bonn, Germany) for help with the mitophagy experiments. This work was funded by the Deutsche Forschungsgemeinschaft (DFG, German Research Foundation) DFG-FOR 2743 (project number 388932620) to D.O.F., W.B., S.G., B.H., P.F.H., and J.H.; DFG project number 414783339 to A.H.; and by the Space Agency at the German Aerospace Center (DLR) on behalf of the German Federal Ministry of Economic Affairs and Climate Action (BMWK grant 50WB2122 to J.H.). A.S. obtained a PhD fellowship from the Research Foundation, Flanders, Belgium (FWO fellowship S35920N). This work was in part supported by the University of Antwerp (TOP-BOF research grant 38694 and GOA research grant 41667 to V.T.), the FWO (research grants G002501 and G040821N to V.T.), and the "Association Belge contre les Maladies Neuromusculaires" (ABMM2019 grant to A.S. and V.T.).

AUTHOR CONTRIBUTIONS

J.O., A.E., S.S., Y.G., and M.F.R. performed molecular biology and cell biology experiments regarding CASA activity and BAG3-mutant variants and analyzed obtained data. A.E. isolated BAG3 complexes by immunoprecipitation for proteomic analysis. H.B. performed mass spectrometry and analysis of proteomics data. S.S. performed fluorescence microscopy and quantification of obtained data. A.J. and A.H. provided tools and designed experiments for RAB protein analysis. D.J., K.S., S.G., and W.B. analyzed human muscle biopsies. T.S. took muscle biopsies from human subjects. B.R., L.L., and B.H. performed cell stretch experiments and corresponding data analysis. A.S. investigated CASA in CMT2 patient cells. P.F.M.v.d.V. and D.O.F. provided tools and designed experiments for analysis of CASA in muscle cells. J.H., Y.G., and M.F.R. performed siRNA experiments, and J.H. performed *in vitro* binding experiments. D.O.F., A.H., W.B., S.G., B.H., V.T., P.F.H., and J.H. performed data analysis, designed experiments, and edited the manuscript. J.H. wrote the publication. All authors edited and approved the manuscript.

DECLARATION OF INTERESTS

The authors declare no competing interests.

Received: January 31, 2024
Revised: June 13, 2024
Accepted: July 26, 2024
Published: August 23, 2024

REFERENCES

1. Hipp, M.S., Kasturi, P., and Hartl, F.U. (2019). The proteostasis network and its decline in ageing. Nat. Rev. Mol. Cell Biol. *20*, 421–435. https://doi.org/10.1038/s41580-019-0101-y.
2. Vilchez, D., Saez, I., and Dillin, A. (2014). The role of protein clearance mechanisms in organismal ageing and age-related diseases. Nat. Commun. *5*, 5659. https://doi.org/10.1038/NCOMMS6659.
3. Höhfeld, J., Benzing, T., Bloch, W., Fürst, D.O., Gehlert, S., Hesse, M., Hoffmann, B., Hoppe, T., Huesgen, P.F., Köhn, M., et al. (2021). Maintaining proteostasis under mechanical stress. EMBO Rep. *22*, e52507. https://doi.org/10.15252/embr.202152507.
4. Tedesco, B., Vendredy, L., Timmerman, V., and Poletti, A. (2023). The chaperone-assisted selective autophagy complex dynamics and dysfunctions. Autophagy *19*, 1619–1641. https://doi.org/10.1080/15548627.2022.2160564.
5. Lei, Z., Brizzee, C., and Johnson, G.V.W. (2015). BAG3 facilitates the clearance of endogenous tau in primary neurons. Neurobiol. Aging *36*, 241–248. https://doi.org/10.1016/j.neurobiolaging.2014.08.012.
6. Ji, C., Tang, M., Zeidler, C., Höhfeld, J., and Johnson, G.V.W. (2019). BAG3 and SYNPO (synaptopodin) facilitate phospho-MAPT/Tau degradation via autophagy in neuronal processes. Autophagy *15*, 1199–1213. https://doi.org/10.1080/15548627.2019.1580096.
7. Crippa, V., Boncoraglio, A., Galbiati, M., Aggarwal, T., Rusmini, P., Giorgetti, E., Cristofani, R., Carra, S., Pennuto, M., and Poletti, A. (2013). Differential autophagy power in the spinal cord and muscle of transgenic ALS mice. Front. Cell. Neurosci. *7*, 234. https://doi.org/10.3389/fncel.2013.00234.
8. Carra, S., Seguin, S.J., Lambert, H., and Landry, J. (2008). HspB8 chaperone activity toward poly(Q)-containing proteins depends on its association with Bag3, a stimulator of macroautophagy. J. Biol. Chem. *283*, 1437–1444. https://doi.org/10.1074/jbc.M706304200.
9. Ulbricht, A., Eppler, F.J., Tapia, V.E., Van Der Ven, P.F.M., Hampe, N., Hersch, N., Vakeel, P., Stadel, D., Haas, A., Saftig, P., et al. (2013). Cellular mechanotransduction relies on tension-induced and chaperone-assisted autophagy. Curr. Biol. *23*, 430–435. https://doi.org/10.1016/j.cub.2013.01.064.

10. Ruparelia, A.A., Oorschot, V., Ramm, G., and Bryson-Richardson, R.J. (2016). FLNC myofibrillar myopathy results from impaired autophagy and protein insufficiency. Hum. Mol. Genet. *25*, 2131–2142. https://doi.org/10.1093/hmg/ddw080.

11. Martin, T.G., Myers, V.D., Dubey, P., Dubey, S., Perez, E., Moravec, C.S., Willis, M.S., Feldman, A.M., and Kirk, J.A. (2021). Cardiomyocyte contractile impairment in heart failure results from reduced BAG3-mediated sarcomeric protein turnover. Nat. Commun. *12*, 2942. https://doi.org/10.1038/s41467-021-23272-z.

12. Arndt, V., Dick, N., Tawo, R., Dreiseidler, M., Wenzel, D., Hesse, M., Fürst, D.O., Saftig, P., Saint, R., Fleischmann, B.K., et al. (2010). Chaperone-Assisted Selective Autophagy Is Essential for Muscle Maintenance. Curr. Biol. *20*, 143–148. https://doi.org/10.1016/j.cub.2009.11.022.

13. Brooks, D., Naeem, F., Stetsiv, M., Goetting, S.C., Bawa, S., Green, N., Clark, C., Bashirullah, A., and Geisbrecht, E.R. (2020). Drosophila NUAK functions with Starvin/BAG3 in autophagic protein turnover. PLoS Genet. *16*, e1008700. https://doi.org/10.1371/journal.pgen.1008700.

14. Ruparelia, A.A., McKaige, E.A., Williams, C., Schulze, K.E., Fuchs, M., Oorschot, V., Lacene, E., Meregalli, M., Lee, C., Serrano, R.J., et al. (2021). Metformin rescues muscle function in BAG3 myofibrillar myopathy models. Autophagy *17*, 2494–2510. https://doi.org/10.1080/15548627.2020.1833500.

15. Homma, S., Iwasaki, M., Shelton, G.D., Engvall, E., Reed, J.C., and Takayama, S. (2006). BAG3 deficiency results in fulminant myopathy and early lethality. Am. J. Pathol. *169*, 761–773. https://doi.org/10.2353/ajpath.2006.060250.

16. Kimura, K., Ooms, A., Graf-Riesen, K., Kuppusamy, M., Unger, A., Schuld, J., Daerr, J., Lother, A., Geisen, C., Hein, L., et al. (2021). Overexpression of human BAG3^{P209L} in mice causes restrictive cardiomyopathy. Nat. Commun. *12*, 3575. https://doi.org/10.1038/s41467-021-23858-7.

17. Selcen, D., Muntoni, F., Burton, B.K., Pegoraro, E., Sewry, C., Bite, A.V., and Engel, A.G. (2009). Mutation in BAG3 causes severe dominant childhood muscular dystrophy. Ann. Neurol. *65*, 83–89. https://doi.org/10.1002/ana.21553.

18. Schänzer, A., Rupp, S., Gräf, S., Zengeler, D., Jux, C., Akintürk, H., Gulatz, L., Mazhari, N., Acker, T., Van Coster, R., et al. (2018). Dysregulated autophagy in restrictive cardiomyopathy due to Pro209Leu mutation in BAG3. Mol. Genet. Metab. *123*, 388–399. https://doi.org/10.1016/j.ymgme.2018.01.001.

19. Savarese, G., Becher, P.M., Lund, L.H., Seferovic, P., Rosano, G.M.C., and Coats, A.J.S. (2023). Global burden of heart failure: a comprehensive and updated review of epidemiology. Cardiovasc. Res. *118*, 3272–3287. https://doi.org/10.1093/CVR/CVAC013.

20. Ulbricht, A., Gehlert, S., Leciejewski, B., Schiffer, T., Bloch, W., and Höhfeld, J. (2015). Induction and adaptation of chaperone-assisted selective autophagy CASA in response to resistance exercise in human skeletal muscle. Autophagy *11*, 538–546. https://doi.org/10.1080/15548627.2015.1017186.

21. Martin, T.G., Tawfik, S., Moravec, C.S., Pak, T.R., and Kirk, J.A. (2021). BAG3 expression and sarcomere localization in the human heart are linked to HSF-1 and are differentially affected by sex and disease. Am. J. Physiol. Heart Circ. Physiol. *320*, H2339–H2350. https://doi.org/10.1152/AJPHEART.00419.2020.

22. Xu, Z., Graham, K., Foote, M., Liang, F., Rizkallah, R., Hurt, M., Wang, Y., Wu, Y., and Zhou, Y. (2013). 14-3-3 protein targets misfolded chaperone-associated proteins to aggresomes. J. Cell Sci. *126*, 4173–4186. https://doi.org/10.1242/jcs.126102.

23. Luthold, C., Lambert, H., Guilbert, S.M., Rodrigue, M.A., Fuchs, M., Varlet, A.A., Fradet-Turcotte, A., and Lavoie, J.N. (2021). CDK1-mediated phosphorylation of BAG3 promotes mitotic cell shape remodeling and the molecular assembly of mitotic p62 bodies. Cells *10*, 2638. https://doi.org/10.3390/cells10102638.

24. Hoffman, N.J., Parker, B.L., Chaudhuri, R., Fisher-Wellman, K.H., Kleinert, M., Humphrey, S.J., Yang, P., Holliday, M., Trefely, S., Fazakerley, D.J., et al. (2015). Global Phosphoproteomic Analysis of Human Skeletal Muscle Reveals a Network of Exercise-Regulated Kinases and AMPK Substrates. Cell Metab. *22*, 922–935. https://doi.org/10.1016/j.cmet.2015.09.001.

25. Potts, G.K., McNally, R.M., Blanco, R., You, J.S., Hebert, A.S., Westphall, M.S., Coon, J.J., and Hornberger, T.A. (2017). A map of the phosphoproteomic alterations that occur after a bout of maximal-intensity contractions. J. Physiol. *595*, 5209–5226. https://doi.org/10.1113/JP273904.

26. Nelson, M.E., Parker, B.L., Burchfield, J.G., Hoffman, N.J., Needham, E.J., Cooke, K.C., Naim, T., Sylow, L., Ling, N.X., Francis, D., et al. (2019). Phosphoproteomics reveals conserved exercise-stimulated signaling and AMPK regulation of store-operated calcium entry. EMBO J. *38*, e102578. https://doi.org/10.15252/embj.2019102578.

27. Orfanos, Z., Gödderz, M.P.O., Soroka, E., Gödderz, T., Rumyantseva, A., Van Der Ven, P.F.M., Hawke, T.J., and Fürst, D.O. (2016). Breaking sarcomeres by in vitro exercise. Sci. Rep. *6*, 19614. https://doi.org/10.1038/srep19614.

28. Lövenich, L., Dreissen, G., Hoffmann, C., Konrad, J., Springer, R., Höhfeld, J., Merkel, R., and Hoffmann, B. (2021). Strain-induced mechanoresponse depends on cell contractility and BAG3-mediated autophagy. Mol. Biol. Cell *32*, ar9. https://doi.org/10.1091/mbc.E21-05-0254.

29. Rauch, J.N., Tse, E., Freilich, R., Mok, S.A., Makley, L.N., Southworth, D.R., and Gestwicki, J.E. (2017). BAG3 Is a Modular, Scaffolding Protein that physically Links Heat Shock Protein 70 (Hsp70) to the Small Heat Shock Proteins. J. Mol. Biol. *429*, 128–141. https://doi.org/10.1016/j.jmb.2016.11.013.

30. Collier, M.P., Alderson, T.R., De Villiers, C.P., Nicholls, D., Gastall, H.Y., Allison, T.M., Degiacomi, M.T., Jiang, H., Mlynek, G., Fürst, D.O., et al. (2019). HspB1 phosphorylation regulates its intramolecular dynamics and mechanosensitive molecular chaperone interaction with filamin C. Sci. Adv. *5*, eaav8421. https://doi.org/10.1126/SCIADV.AAV8421.

31. Grosshans, B.L., Ortiz, D., and Novick, P. (2006). Rabs and their effectors: achieving specificity in membrane traffic. Proc. Natl. Acad. Sci. USA *103*, 11821–11827. https://doi.org/10.1073/PNAS.0601617103.

32. Jäger, S., Bucci, C., Tanida, I., Ueno, T., Kominami, E., Saftig, P., and Eskelinen, E.L. (2004). Role for Rab7 in maturation of late autophagic vacuoles. J. Cell Sci. *117*, 4837–4848. https://doi.org/10.1242/jcs.01370.

33. Yan, B.R., Li, T., Coyaud, E., Laurent, E.M.N., St-Germain, J., Zhou, Y., Kim, P.K., Raught, B., and Brumell, J.H. (2022). C5orf51 is a component of the MON1-CCZ1 complex and controls RAB7A localization and stability during mitophagy. Autophagy *18*, 829–840. https://doi.org/10.1080/15548627.2021.1960116.

34. Li, Z., Schulze, R.J., Weller, S.G., Krueger, E.W., Schott, M.B., Zhang, X., Casey, C.A., Liu, J., Stöckli, J., James, D.E., et al. (2016). A novel Rab10-EHBP1-EHD2 complex essential for the autophagic engulfment of lipid droplets. Sci. Adv. *2*, e1601470. https://doi.org/10.1126/SCIADV.1601470.

35. Ding, X., Jiang, X., Tian, R., Zhao, P., Li, L., Wang, X., Chen, S., Zhu, Y., Mei, M., Bao, S., et al. (2019). RAB2 regulates the formation of autophagosome and autolysosome in mammalian cells. Autophagy *15*, 1774–1786. https://doi.org/10.1080/15548627.2019.1596478.

36. Webster, C.P., Smith, E.F., Bauer, C.S., Moller, A., Hautbergue, G.M., Ferraiuolo, L., Myszczynska, M.A., Higginbottom, A., Walsh, M.J., Whitworth, A.J., et al. (2016). The C9orf72 protein interacts with Rab1a and the ULK1 complex to regulate initiation of autophagy. EMBO J. *35*, 1656–1676. https://doi.org/10.15252/EMBJ.201694401.

37. Kakuta, S., Yamaguchi, J., Suzuki, C., Sasaki, M., Kazuno, S., and Uchiyama, Y. (2017). Small GTPase Rab1B is associated with ATG9A vesicles and regulates autophagosome formation. FASEB J. *31*, 3757–3773. https://doi.org/10.1096/fj.201601052R.

38. Wauters, F., Cornelissen, T., Imberechts, D., Martin, S., Koentjoro, B., Sue, C., Vangheluwe, P., and Vandenberghe, W. (2020). LRRK2 mutations impair depolarization-induced mitophagy through inhibition of mitochondrial accumulation of RAB10. Autophagy *16*, 203–222. https://doi.org/10.1080/15548627.2019.1603548.

39. Puri, C., Vicinanza, M., Ashkenazi, A., Gratian, M.J., Zhang, Q., Bento, C.F., Renna, M., Menzies, F.M., and Rubinsztein, D.C. (2018). The RAB11A-Positive Compartment Is a Primary Platform for Autophagosome Assembly Mediated by WIPI2 Recognition of PI3P-RAB11A. Dev. Cell *45*, 114–131.e8. https://doi.org/10.1016/j.devcel.2018.03.008.

40. Winslow, A.R., Chen, C.W., Corrochano, S., Acevedo-Arozena, A., Gordon, D.E., Peden, A.A., Lichtenberg, M., Menzies, F.M., Ravikumar, B., Imarisio, S., et al. (2010). αSynuclein impairs macroautophagy: Implications for Parkinson's disease. J. Cell Biol. *190*, 1023–1037. https://doi.org/10.1083/jcb.201003122.

41. Yaffe, D., and Saxel, O. (1977). Serial passaging and differentiation of myogenic cells isolated from dystrophic mouse muscle. Nature *270*, 725–727. https://doi.org/10.1038/270725a0.

42. Spinosa, M.R., Progida, C., De Luca, A., Colucci, A.M.R., Alifano, P., and Bucci, C. (2008). Functional characterization of Rab7 mutant proteins associated with Charcot-Marie-Tooth type 2B disease. J. Neurosci. *28*, 1640–1648. https://doi.org/10.1523/JNEUROSCI.3677-07.2008.

43. Gutierrez, M.G., Munafó, D.B., Berón, W., and Colombo, M.I. (2004). Rab7 is required for the normal progression of the autophagic pathway in mammalian cells. J. Cell Sci. *117*, 2687–2697. https://doi.org/10.1242/jcs.01114.

44. Stroupe, C. (2018). This Is the End: Regulation of Rab7 Nucleotide Binding in Endolysosomal Trafficking and Autophagy. Front. Cell Dev. Biol. *6*, 129. https://doi.org/10.3389/FCELL.2018.00129.

45. Körschgen, H., Baeken, M., Schmitt, D., Nagel, H., and Behl, C. (2023). Co-chaperone BAG3 enters autophagic pathway via its interaction with microtubule associated protein 1 light chain 3 beta. Traffic *24*, 564–575. https://doi.org/10.1111/tra.12916.

46. Zellner, S., Schifferer, M., and Behrends, C. (2021). Systematically defining selective autophagy receptor-specific cargo using autophagosome content profiling. Mol. Cell *81*, 1337–1354.e8. https://doi.org/10.1016/j.molcel.2021.01.009.

47. Heo, J.M., Ordureau, A., Swarup, S., Paulo, J.A., Shen, K., Sabatini, D.M., and Harper, J.W. (2018). RAB7A phosphorylation by TBK1 promotes mitophagy via the PINK-PARKIN pathway. Sci. Adv. *4*, eaav0443. https://doi.org/10.1126/sciadv.aav0443.

48. Tahrir, F.G., Knezevic, T., Gupta, M.K., Gordon, J., Cheung, J.Y., Feldman, A.M., and Khalili, K. (2017). Evidence for the Role of BAG3 in Mitochondrial Quality Control in Cardiomyocytes. J. Cell. Physiol. *232*, 797–805. https://doi.org/10.1002/JCP.25476.

49. Matsuda, N., Sato, S., Shiba, K., Okatsu, K., Saisho, K., Gautier, C.A., Sou, Y.S., Saiki, S., Kawajiri, S., Sato, F., et al. (2010). PINK1 stabilized by mitochondrial depolarization recruits Parkin to damaged mitochondria and activates latent Parkin for mitophagy. J. Cell Biol. *189*, 211–221. https://doi.org/10.1083/jcb.200910140.

50. Rakovic, A., Ziegler, J., Mårtensson, C.U., Prasuhn, J., Shurkewitsch, K., König, P., Paulson, H.L., and Klein, C. (2019). PINK1-dependent mitophagy is driven by the UPS and can occur independently of LC3 conversion. Cell Death Differ. *26*, 1428–1441. https://doi.org/10.1038/s41418-018-0219-z.

51. Koyano, F., Okatsu, K., Kosako, H., Tamura, Y., Go, E., Kimura, M., Kimura, Y., Tsuchiya, H., Yoshihara, H., Hirokawa, T., et al. (2014). Ubiquitin is phosphorylated by PINK1 to activate parkin. Nature *510*, 162–166. https://doi.org/10.1038/nature13392.

52. Haidar, M., Asselbergh, B., Adriaenssens, E., De Winter, V., Timmermans, J.P., Auer-Grumbach, M., Juneja, M., and Timmerman, V. (2019). Neuropathy-causing mutations in HSPB1 impair autophagy by disturbing the formation of SQSTM1/p62 bodies. Autophagy *15*, 1051–1068. https://doi.org/10.1080/15548627.2019.1569930.

53. Alderson, T.R., Adriaenssens, E., Asselbergh, B., Pritišanac, I., Van Lent, J., Gastall, H.Y., Wälti, M.A., Louis, J.M., Timmerman, V., Baldwin, A.J., et al. (2021). A weakened interface in the P182L variant of HSP27 associated with severe Charcot-Marie-Tooth neuropathy causes aberrant binding to interacting proteins. EMBO J. *40*, e103811. https://doi.org/10.15252/EMBJ.2019103811.

54. Tedesco, B., Vendredy, L., Adriaenssens, E., Cozzi, M., Asselbergh, B., Crippa, V., Cristofani, R., Rusmini, P., Ferrari, V., Casarotto, E., et al. (2023). HSPB8 frameshift mutant aggregates weaken chaperone-assisted selective autophagy in neuromyopathies. Autophagy *19*, 2217–2239. https://doi.org/10.1080/15548627.2023.2179780.

55. Romano, R., Rivellini, C., De Luca, M., Tonlorenzi, R., Beli, R., Manganelli, F., Nolano, M., Santoro, L., Eskelinen, E.L., Previtali, S.C., et al. (2021). Alteration of the late endocytic pathway in Charcot–Marie–Tooth type 2B disease. Cell. Mol. Life Sci. *78*, 351–372. https://doi.org/10.1007/s00018-020-03510-1.

56. Adriaenssens, E., Tedesco, B., Mediani, L., Asselbergh, B., Crippa, V., Antoniani, F., Carra, S., Poletti, A., and Timmerman, V. (2020). BAG3 Pro209 mutants associated with myopathy and neuropathy relocate chaperones of the CASA-complex to aggresomes. Sci. Rep. *10*, 8755. https://doi.org/10.1038/s41598-020-65664-z.

57. Fu, J., Ma, M., Song, J., Pang, M., Li, G., and Zhang, J. (2020). BAG3 p.Pro209Ser mutation identified in a Chinese family with Charcot-Marie-Tooth disease. J. Neurol. *267*, 1080–1085. https://doi.org/10.1007/s00415-019-09680-8.

58. Shy, M., Rebelo, A.P., Feely, S.M., Abreu, L.A., Tao, F., Swenson, A., Bacon, C., and Zuchner, S. (2018). Mutations in BAG3 cause adult-onset Charcot-Marie-Tooth disease. J. Neurol. Neurosurg. Psychiatry *89*, 313–315. https://doi.org/10.1136/jnnp-2017-315929.

59. Mulligan, R.J., and Winckler, B. (2023). Regulation of Endosomal Trafficking by Rab7 and Its Effectors in Neurons: Clues from Charcot–Marie–Tooth 2B Disease. Biomolecules *13*, 1399. https://doi.org/10.3390/biom13091399.

60. Verhoeven, K., De Jonghe, P., Coen, K., Verpoorten, N., Auer-Grumbach, M., Kwon, J.M., FitzPatrick, D., Schmedding, E., De Vriendt, E., Jacobs, A., et al. (2003). Mutations in the small GTP-ase late endosomal protein RAB7 cause Charcot-Marie-Tooth type 2B neuropathy. Am. J. Hum. Genet. *72*, 722–727. https://doi.org/10.1086/367847.

61. McCray, B.A., Skordalakes, E., and Taylor, J.P. (2010). Disease mutations in Rab7 result in unregulated nucleotide exchange and inappropriate activation. Hum. Mol. Genet. *19*, 1033–1047. https://doi.org/10.1093/hmg/ddp567.

62. Fuchs, M., Poirier, D.J., Seguin, S.J., Lambert, H., Carra, S., Charette, S.J., and Landry, J. (2009). Identification of the key structural motifs involved in HspB8/HspB6-Bag3 interaction. Biochem. J. *425*, 245–255. https://doi.org/10.1042/BJ20090907.

63. Carra, S., Alberti, S., Arrigo, P.A., Benesch, J.L., Benjamin, I.J., Boelens, W., Bartelt-Kirbach, B., Brundel, B.J.J.M., Buchner, J., Bukau, B., et al. (2017). The growing world of small heat shock proteins: from structure to functions. Cell Stress Chaperones *22*, 601–611. https://doi.org/10.1007/s12192-017-0787-8.

64. Guilbert, S.M., Lambert, H., Rodrigue, M.A., Fuchs, M., Landry, J., and Lavoie, J.N. (2018). Hspb8 and bag3 cooperate to promote spatial sequestration of ubiquitinated proteins and coordinate the cellular adaptive response to proteasome insufficiency. FASEB J. *32*, 3518–3535. https://doi.org/10.1096/fj.201700558RR.

65. Ganassi, M., Mateju, D., Bigi, I., Mediani, L., Poser, I., Lee, H.O., Seguin, S.J., Morelli, F.F., Vinet, J., Leo, G., et al. (2016). A Surveillance Function of the HSPB8-BAG3-HSP70 Chaperone Complex Ensures Stress Granule Integrity and Dynamism. Mol. Cell *63*, 796–810. https://doi.org/10.1016/j.molcel.2016.07.021.

66. Tremel, S., Ohashi, Y., Morado, D.R., Bertram, J., Perisic, O., Brandt, L.T.L., von Wrisberg, M.K., Chen, Z.A., Maslen, S.L., Kovtun, O., et al. (2021). Structural basis for VPS34 kinase activation by rab1 and Rab5 on membranes. Nat. Commun. *12*, 1564. https://doi.org/10.1038/s41467-021-21695-2.

67. Longatti, A., Lamb, C.A., Razi, M., Yoshimura, S.I., Barr, F.A., and Tooze, S.A. (2012). TBC1D14 regulates autophagosome formation via Rab11- and ULK1-positive recycling endosomes. J. Cell Biol. *197*, 659–675. https://doi.org/10.1083/jcb.201111079.

68. Lapierre, L.A., Dorn, M.C., Zimmerman, C.F., Navarre, J., Burnette, J.O., and Goldenring, J.R. (2003). Rab11b resides in a vesicular compartment distinct from Rab11a in parietal cells and other epithelial cells. Exp. Cell Res. *290*, 322–331. https://doi.org/10.1016/S0014-4827(03)00340-9.

69. Grimsey, N.J., Coronel, L.J., Cordova, I.C., and Trejo, J. (2016). Recycling and endosomal sorting of protease-activated receptor-1 is distinctly regulated by Rab11A and Rab11B proteins. J. Biol. Chem. *291*, 2223–2236. https://doi.org/10.1074/jbc.M115.702993.

70. Scapin, S.M.N., Carneiro, F.R.G., Alves, A.C., Medrano, F.J., Guimarães, B.G., and Zanchin, N.I.T. (2006). The crystal structure of the small GTPase Rab11b reveals critical differences relative to the Rab11a isoform. J. Struct. Biol. *154*, 260–268. https://doi.org/10.1016/j.jsb.2006.01.007.

71. Howe, E.N., Burnette, M.D., Justice, M.E., Schnepp, P.M., Hedrick, V., Clancy, J.W., Guldner, I.H., Lamere, A.T., Li, J., Aryal, U.K., et al. (2020). Rab11b-mediated integrin recycling promotes brain metastatic adaptation and outgrowth. Nat. Commun. *11*, 3017. https://doi.org/10.1038/s41467-020-16832-2.

72. Thant, L., Kakihara, Y., Kaku, M., Kitami, M., Kitami, K., Mizukoshi, M., Maeda, T., Saito, I., and Saeki, M. (2022). Involvement of Rab11 in osteoblastic differentiation: Its up-regulation during the differentiation and by tensile stress. Biochem. Biophys. Res. Commun. *624*, 16–22. https://doi.org/10.1016/j.bbrc.2022.07.061.

73. Kimura, S., Noda, T., and Yoshimori, T. (2007). Dissection of the autophagosome maturation process by a novel reporter protein, tandem fluorescent-tagged LC3. Autophagy *3*, 452–460. https://doi.org/10.4161/auto.4451.

74. Hegedűs, K., Takáts, S., Boda, A., Jipa, A., Nagy, P., Varga, K., Kovács, A.L., and Juhász, G. (2016). The Ccz1-Mon1-Rab7 module and Rab5 control distinct steps of autophagy. Mol. Biol. Cell *27*, 3132–3142. https://doi.org/10.1091/mbc.E16-03-0205.

75. Wang, Z., Miao, G., Xue, X., Guo, X., Yuan, C., Wang, Z., Zhang, G., Chen, Y., Feng, D., Hu, J., et al. (2016). The Vici Syndrome Protein EPG5 Is a Rab7 Effector that Determines the Fusion Specificity of Autophagosomes with Late Endosomes/Lysosomes. Mol. Cell *63*, 781–795. https://doi.org/10.1016/j.molcel.2016.08.021.

76. Lin, H., Tang, M., Ji, C., Girardi, P., Cvetojevic, G., Chen, D., Koren, S.A., and Johnson, G.V.W. (2022). BAG3 Regulation of RAB35 Mediates the Endosomal Sorting Complexes Required for Transport/Endolysosome Pathway and Tau Clearance. Biol. Psychiatry *92*, 10–24. https://doi.org/10.1016/j.biopsych.2021.10.024.

77. Yamano, K., Wang, C., Sarraf, S.A., Münch, C., Kikuchi, R., Noda, N.N., Hizukuri, Y., Kanemaki, M.T., Harper, W., Tanaka, K., et al. (2018). Endosomal Rab cycles regulate parkin-mediated mitophagy. eLife *7*, e31326. https://doi.org/10.7554/eLife.31326.

78. Nordmann, M., Cabrera, M., Perz, A., Bröcker, C., Ostrowicz, C., Engelbrecht-Vandré, S., and Ungermann, C. (2010). The Mon1-Ccz1 complex is the GEF of the late endosomal Rab7 homolog Ypt7. Curr. Biol. *20*, 1654–1659. https://doi.org/10.1016/j.cub.2010.08.002.

79. Kiontke, S., Langemeyer, L., Kuhlee, A., Schuback, S., Raunser, S., Ungermann, C., and Kümmel, D. (2017). Architecture and mechanism of the late endosomal Rab7-like Ypt7 guanine nucleotide exchange factor complex Mon1-Ccz1. Nat. Commun. *8*, 14034. https://doi.org/10.1038/ncomms14034.

80. Kleine Balderhaar, H.J., and Ungermann, C. (2013). CORVET and HOPS tethering complexes – coordinators of endosome and lysosome fusion. J. Cell Sci. *126*, 1307–1316. https://doi.org/10.1242/jcs.107805.

81. Chen, C.C.W., Erlich, A.T., Crilly, M.J., and Hood, D.A. (2018). Parkin is required for exercise-induced mitophagy in muscle: Impact of aging. Am. J. Physiol. Endocrinol. Metab. *315*, E404–E415. https://doi.org/10.1152/ajpendo.00391.2017.

82. Erlich, A.T., and Hood, D.A. (2019). Mitophagy Regulation in Skeletal Muscle: Effect of Endurance Exercise and Age. J. Sci. Sport Exer. *1*, 228–236. https://doi.org/10.1007/s42978-019-00041-5.

83. Guo, C., Wu, R.-Y., Dou, J.-H., Song, S.-F., Sun, X.-L., Hu, Y.-W., Guo, F.-S., Wei, J., Lin, L., and Wei, J. (2023). Mitophagy-dependent Cardioprotection of Resistance Training on Heart Failure. J. Appl. Physiol. (1985) *135*, 1390–1401. https://doi.org/10.1152/JAPPLPHYSIOL.00674.2023.

84. Wang, J., Tomar, D., Martin, T.G., Dubey, S., Dubey, P.K., Song, J., Landesberg, G., McCormick, M.G., Myers, V.D., Merali, S., et al. (2023). Bag3 Regulates Mitochondrial Function and the Inflammasome Through Canonical and Noncanonical Pathways in the Heart. JACC Basic Transl. Sci. *8*, 820–839. https://doi.org/10.1016/j.jacbts.2022.12.013.

85. Meggouh, F., Bienfait, H.M.E., Weterman, M.A.J., De Visser, M., and Baas, F. (2006). Charcot-Marie-Tooth disease due to a de novo mutation of the RAB7 gene. Neurology *67*, 1476–1478. https://doi.org/10.1212/01.WNL.0000240068.21499.F5.

86. Saveri, P., De Luca, M., Nisi, V., Pisciotta, C., Romano, R., Piscosquito, G., Reilly, M.M., Polke, J.M., Cavallaro, T., Fabrizi, G.M., et al. (2020). Charcot-Marie-Tooth Type 2B: A New Phenotype Associated with a Novel RAB7A Mutation and Inhibited EGFR Degradation. Cells *9*, 1028. https://doi.org/10.3390/cells9041028.

87. Linnemann, A., van der Ven, P.F.M., Vakeel, P., Albinus, B., Simonis, D., Bendas, G., Schenk, J.A., Micheel, B., Kley, R.A., and Fürst, D.O. (2010). The sarcomeric Z-disc component myopodin is a multiadapter protein that interacts with filamin and α-actinin. Eur. J. Cell Biol. *89*, 681–692. https://doi.org/10.1016/j.ejcb.2010.04.004.

88. Schleinitz, A., Pöttgen, L.A., Keren-Kaplan, T., Pu, J., Saftig, P., Bonifacino, J.S., Haas, A., and Jeschke, A. (2023). Consecutive functions of small GTPases guide HOPS-mediated tethering of late endosomes and lysosomes. Cell Rep. *42*, 111969. https://doi.org/10.1016/j.celrep.2022.111969.

89. Pankiv, S., Clausen, T.H., Lamark, T., Brech, A., Bruun, J.A., Outzen, H., Øvervatn, A., Bjørkøy, G., and Johansen, T. (2007). p62/SQSTM1 binds directly to Atg8/LC3 to facilitate degradation of ubiquitinated protein aggregates by autophagy*. J. Biol. Chem. *282*, 24131–24145. https://doi.org/10.1074/jbc.M702824200.

90. Tyanova, S., Temu, T., and Cox, J. (2016). The MaxQuant computational platform for mass spectrometry-based shotgun proteomics. Nat. Protoc. *11*, 2301–2319. https://doi.org/10.1038/nprot.2016.136.

91. Yu, S.H., Ferretti, D., Schessner, J.P., Rudolph, J.D., Borner, G.H.H., and Cox, J. (2020). Expanding the Perseus Software for Omics Data Analysis With Custom Plugins. Curr. Protoc. Bioinformatics *71*, e105. https://doi.org/10.1002/cpbi.105.

92. Gu, Z., Eils, R., and Schlesner, M. (2016). Complex heatmaps reveal patterns and correlations in multidimensional genomic data. Bioinformatics *32*, 2847–2849. https://doi.org/10.1093/bioinformatics/btw313.

93. Ge, S.X., Jung, D., and Yao, R. (2020). ShinyGO: A graphical gene-set enrichment tool for animals and plants. Bioinformatics *36*, 2628–2629. https://doi.org/10.1093/bioinformatics/btz931.

94. Schneider, C.A., Rasband, W.S., and Eliceiri, K.W. (2012). NIH Image to ImageJ: 25 years of image analysis. Nat. Methods *9*, 671–675. https://doi.org/10.1038/nmeth.2089.

95. Faust, U., Hampe, N., Rubner, W., Kirchgessner, N., Safran, S., Hoffmann, B., and Merkel, R. (2011). Cyclic stress at mHz frequencies aligns fibroblasts in direction of zero strain. PLoS One *6*, e28963. https://doi.org/10.1371/journal.pone.0028963.

96. Bucci, C., Thomsen, P., Nicoziani, P., McCarthy, J., and Van Deurs, B. (2000). Rab7: A key to lysosome biogenesis. Mol. Biol. Cell *11*, 467–480. https://doi.org/10.1091/mbc.11.2.467.

Please cite this article in press as: Ottensmeyer et al., Force-induced dephosphorylation activates the cochaperone BAG3 to coordinate protein homeostasis and membrane traffic, Current Biology (2024), https://doi.org/10.1016/j.cub.2024.07.088

STAR★METHODS

KEY RESOURCES TABLE

REAGENT or RESOURCE	SOURCE	IDENTIFIER
Antibodies		
Rabbit polyclonal anti-BAG3	Proteintech	Cat#: 10599-1-AP; RRID: AB_2062602
Rabbit polyclonal anti-BAG3	Arndt et al.[12]	N/A
Rabbit polyclonal anti-BAG3-pS136	This paper	N/A
Rabbit polyclonal anti-HSC70	Ulbricht et al.[9]	N/A
Rabbit polyclonal anti-HSPB1	Enzo	Cat#: ADI-SPA-801; RRID: AB_10615795
Rabbit polyclonal anti-HSPB8	St Johnś Lab	Cat#: STJ24102
Rabbit polyclonal anti-LC3B	Novus Biologicals	Cat#: NB100-2220; RRID: AB_10003146
Rabbit polyclonal anti-RAB2A	Proteintech	Cat#: 15420-1-AP; RRID: AB_2176874
Rabbit polyclonal anti-RAB7A	T. Watts (University of Toronto, Canada)	N/A
Rabbit polyclonal anti-RAB11A	Abcam	Cat#: Ab128913; RRID: AB_11140633
Rabbit polyclonal anti-RAB11B	Proteintech	Cat#: 19742-1-AP; RRID: AB_10642010
Guinea pig polyclonal anti-SQSTM1/p62	Progen	Cat#: GP62-C; RRID: AB_2687531
Rabbit polyclonal anti-SYNPO2	Linnemann et al.[87]	N/A
Mouse monoclonal anti-T7	Sigma-Aldrich	Cat#: 69522
Mouse monoclonal anti-γ-tubulin	Sigma-Aldrich	Cat#: T5326; RRID: AB_532292
Rabbit polyclonal anti-ubiquitin-pS65	Cell Signaling	Cat#: 62802; RRID: AB_2799632
Bacterial and virus strains		
Escherichia coli BL21(DE3)	Thermo Fisher	Cat#: ECO114
Biological samples		
Human vastus lateralis muscle biopsies	This paper	N/A
Chemicals, peptides, and recombinant proteins		
Cell lysis buffer	Cell Signaling Technology	Cat#: 9803
Protease-Inhibitor-Cocktail	Thermo Fisher	Cat#: 78429
Complete protease inhibitor	Roche	Cat#: 4693132001
PhosSTOP phosphatase inhibitor	Roche	Cat#: 4906837001
RIPA buffer	Thermo Fisher	Cat#: 89901
Protease inhibitor cocktail	Sigma-Aldrich	Cat#: P8340
Phosphatase inhibitor cocktail	Sigma-Aldrich	Cat#: P5726
M2-agarose	Sigma-Aldrich	Cat#: A2220
Cycloheximide	Roth	Cat#: 8682.1
Anti-FLAG magnetic beads	Thermo Fisher	Cat#: A36797
SDS, proteomics grade	VWR	Cat#: M112
Bafilomycin A1	Santa Cruz Biotechnology	Cat#: sc-201550A
Fluoromount-G	Thermo Fisher	Cat#: 00-4958-02
Ni-NTA-agarose	Qiagen	Cat#: 30210
GDP	Merck	Cat#: 20-177
GTP-γ-S	Merck	Cat#: 20-176
Protein G sepharose	Sigma-Aldrich	Cat#: GE17-0618-01

(*Continued on next page*)

Please cite this article in press as: Ottensmeyer et al., Force-induced dephosphorylation activates the cochaperone BAG3 to coordinate protein homeostasis and membrane traffic, Current Biology (2024), https://doi.org/10.1016/j.cub.2024.07.088

Continued

REAGENT or RESOURCE	SOURCE	IDENTIFIER
CCCP	Sigma-Aldrich	Cat#: C2759
Valinomycin	Sigma-Aldrich	Cat#: 94675
PQRSQpSPLRG (phosphopeptide of human BAG3 (aa 131 – 140) for anti-BAG3-pS136 antibody generation)	Eurogentec	N/A
PQRSQSPLRG (control peptide for anti-BAG3-pS136 antibody purification)	Eurogentec	N/A
λ-phosphatase	New England Biolabs	Cat#: P0753
Fibronectin	Corning or Sigma-Aldrich	Cat#: 356008 (Corning); F2006 (Sigma-Aldrich)
BAG3-T285A/S289A	This paper	N/A
BAG3	This paper	N/A
T7-RAB7A	This paper	N/A
LC3B	This paper	N/A
Critical commercial assays		
Precellys lysing kits CKMix	Bertin Instruments	Cat#: P000918-LYSKO-A.0
Pierce Bradford protein assay kit	Thermo Fisher	Cat#: 23225
Bradford protein assay dye	Bio-Rad	Cat#: 5000006
CalPhos transfection kit	Clontech	Cat#: 631312
JetPRIME transfection reagent	Polyplus	Cat#: 101000001
μPAC reverse phase trap column	Thermo Fisher	Cat#: COL-TRPNANO16G1B2
μPAC reverse phase analytical column	Thermo Fisher	Cat#: COL-NANO050G1B
Deposited data		
Differential interactome proteomics of BAG3 phosphosite mutant variants	This paper	PRIDE: PXD048551
Experimental models: Cell lines		
Human: HeLa	Sigma-Aldrich	Cat#: 93021013
Rat: A7r5	Sigma-Aldrich	Cat#: 86050803
Mouse: C2C12	Sigma-Aldrich	Cat#: 91031101
Mouse: C2	D. Fürst (University of Bonn, Germany)	N/A
Lymphoid cell lines of CMT2 patient and unaffected relative	This paper	N/A
Oligonucleotides		
BAG3-S136A – forward 5'-CCT CAG AGG TCC CAG GCA CCT CTG CGG GGC A-3'	This paper	N/A
BAG3-S136A – reverse 5'-TGC CCC GCA GAG GTG CCT GGG ACC TCT GAG G-3'	This paper	N/A
BAG3-S136D – forward 5'-CTC AGA GGT CCC AGG ACC CTC TGC GGG GCA TG-3'	This paper	N/A
BAG3-S136D – reverse 5'-CAT GCC CCG CAG AGG GTC CTG GGA CCT CTG AG-3'-	This paper	N/A
BAG3-S264A – forward 5'-CCC CTG CGG GCG GCA GCC CCG TTC AGG TCA T-3'	This paper	N/A
BAG3-S264A – reverse 5'-ATG ACC TGA ACG GGG CTG CCG CCC GCA GGG G-3'	This paper	N/A

(*Continued on next page*)

Continued

REAGENT or RESOURCE	SOURCE	IDENTIFIER
BAG3-S264D – forward 5'-CCC CTG CGG GCG GCA GAC CCG TTC AGG TCA TC-3'	This paper	N/A
BAG3-S264D – reverse 5'-GAT GAC CTG AAC GGG TCT GCC GCC CGC AGG GG-3'	This paper	N/A
BAG3-S275A – forward 5'-CAG GGT GCA TCG GCC CGG GAG GGC TCA -3'	This paper	N/A
BAG3-S275A – reverse 5'-TGA GCC CTC CCG GGC CGA TGC ACC CTG -3'	This paper	N/A
BAG3-S275D – forward 5'-GTC CAG GGT GCA TCG GAC CGG GAG GGC TCA -3'	This paper	N/A
BAG3-S275D – reverse 5'-TGA GCC CTC CCG GTC CGA TGC ACC CTG GAC -3	This paper	N/A
BAG3-S279A – forward 5'-TCG AGC CGG GAG GGC GCA CCA GCC AGG AGC A-3'	This paper	N/A
BAG3-S279A – reverse 5'-TGC TCC TGG CTG GTG CGC CCT CCC GGC TCG A-3'	This paper	N/A
BAG3-S279D – forward 5'-CGA GCC GGG AGG GCG ACC CAG CCA GGA GCA GC-3'	This paper	N/A
BAG3-S279D – reverse 5'-GCT GCT CCT GGC TGG GTC GCC CTC CCG GCT CG-3'	This paper	N/A
BAG3-T285A – forward 5'-CCA GCC AGG AGC AGC GCG CCA CTC CAC TCC C-3'	This paper	N/A
BAG3-T285A – reverse 5'-GGG AGT GGA GTG GCG CGC TGC TCC TGG CTG G-3'	This paper	N/A
BAG3-T285D – forward 5'-CAG CCA GGA GCA GCG ACC CAC TCC ACT CCC CC-3'	This paper	N/A
BAG3-T285D – reverse 5'-GGG GGA GTG GAG TGG GTC GCT GCT CCT GGC TG-3'	This paper	N/A
BAG3-T285A/S289A – forward 5'-AGC GCG CCA CTC CAC GCC CCC TCG CCC ATC C-3'	This paper	N/A
BAG3-T285A/S289A – reverse 5'-GGA TGG GCG AGG GGG CGT GGA GTG GCG CGC T-3'	This paper	N/A
BAG3-T285D/S289D – forward 5'-AGC GAC CCA CTC CAC GAC CCC TCG CCC ATC CG-3'	This paper	N/A
BAG3-T285D/S289D – reverse 5'-CGG ATG GGC GAG GGG TCG TGG AGT GGG TCG CT-3'	This paper	N/A
BAG3-S289A – forward 5'-AGC ACG CCA CTC CAC GCC CCC TCG CCC ATC C-3'	This paper	N/A

(*Continued on next page*)

Please cite this article in press as: Ottensmeyer et al., Force-induced dephosphorylation activates the cochaperone BAG3 to coordinate protein homeostasis and membrane traffic, Current Biology (2024), https://doi.org/10.1016/j.cub.2024.07.088

Continued

REAGENT or RESOURCE	SOURCE	IDENTIFIER
BAG3-S289A – reverse 5'-GGA TGG GCG AGG GGG CGT GGA GTG GCG TGC T-3	This paper	N/A
BAG3-S289D – forward 5'-GCA CGC CAC TCC ACG ACC CCT CGC CCA TCC G-3'	This paper	N/A
BAG3-S289D – reverse 5'-CGG ATG GGC GAG GGG TCG TGG AGT GGC GTG C-3'	This paper	N/A
MISSION siRNA-Universal-Negativkontrolle Nr. 1	Sigma-Aldrich	Cat#: SIC001
MISSION siRNA against rat HSPB1: 5'-CCAAGGAAGGCG UGGUGGA[dT][dT]-3'	Sigmal-Aldrich	Cat#: SASI_Rn01_00093719
Custom siRNA against mouse RAB2A: 5'-GAAGGAGUCUUU GACAUUA[dT][dT]-3'	Schleinitz et al.[88]	N/A
Custom siRNA against mouse RAB7A: 5'-CCAUCAAACUGGACAAGAA[dT][dT]-3'	Schleinitz et al.[88]	N/A
MISSION siRNA against mouse RAB11A: 5'-GUCAGAACAUCUA AGGCGU[dT][dT]-3'	Sigma-Aldrich	Cat#: SASI_Mm01_00108290
MISSION siRNA against mouse RAB11B: 5'-CACCUUCGGGCUGUG CCCA[dT][dT]-3'	Sigma-Aldrich	Cat#: SASI_Mm02_00315111
Recombinant DNA		
pCMV-Tag2B-BAG3	Arndt et al.[12]	N/A
pCMV-Tag2B-BAG3-S136A	This paper	N/A
pCMV-Tag2B-BAG3-S136D	This paper	N/A
pCMV-Tag2B-BAG3-S264A	This paper	N/A
pCMV-Tag2B-BAG3-S264D	This paper	N/A
pCMV-Tag2B-BAG3-S275A	This paper	N/A
pCMV-Tag2B-BAG3-S275D	This paper	N/A
pCMV-Tag2B-BAG3-S279A	This paper	N/A
pCMV-Tag2B-BAG3-S279D	This paper	N/A
pCMV-Tag2B-BAG3-T285A	This paper	N/A
pCMV-Tag2B-BAG3-T285D	This paper	N/A
pCMV-Tag2B-BAG3-T285A/S289A	This paper	N/A
pCMV-Tag2B-BAG3-T285D/S289D	This paper	N/A
pCMV-Tag2B-BAG3-S289A	This paper	N/A
pCMV-Tag2B-BAG3-S289D	This paper	N/A
mCherry-EGFP-LC3B	Pankiv et al.[89]	N/A
pcDNA3.1-RAB7A-T22N	This paper	N/A
pETM11-BAG3	Kimura et al.[16]	N/A
pETM11-BAG3-T285A/S289A	This paper	N/A
pET28a-RAB7A	This paper	N/A
pET23-EEF-LC3B	This paper	N/A
Software and algorithms		
HyStar	Bruker	https://www.bruker.com/en/products-and-solutions/mass-spectrometry/lc-ms/compass-hystar.html
MaxQuant	Tyanova et al.[90]	https://www.maxquant.org/

(*Continued on next page*)

Please cite this article in press as: Ottensmeyer et al., Force-induced dephosphorylation activates the cochaperone BAG3 to coordinate protein homeostasis and membrane traffic, Current Biology (2024), https://doi.org/10.1016/j.cub.2024.07.088

Continued

REAGENT or RESOURCE	SOURCE	IDENTIFIER
Perseus	Tyanova et al.[90]	https://maxquant.net/perseus/
LIMMA R package plugin within Perseus	Yu et al.[91]	https://support.bioconductor.org/p/2536/
ComplexHeatmaps	Gu et al.[92]	https://bioconductor.org/packages/release/bioc/html/ComplexHeatmap.html
EnhancedVolcano	https://github.com/kevinblighe/EnhancedVolcano	https://github.com/kevinblighe/EnhancedVolcano
ShinyGO	Ge et al.[93]	http://bioinformatics.sdstate.edu/go/
ImageJ	Schneider et al.[94]	https://imagej.nih.gov/ij/
GraphPad Prism	Graphpad	https://www.graphpad.com/

RESOURCE AVAILABILITY

Lead contact

Further information and requests for resources and reagents should be directed to and will be fulfilled by the lead contact, Jörg Höhfeld (hoehfeld@uni-bonn.de).

Materials availability

Newly generated materials described in this paper are available upon request.

Data and code availability

- Proteomics data have been deposited at the PRIDE repository. Accession number is listed in the key resources table.
- Non-standardized data reported in this paper will be shared by the lead contact upon request.
- This paper does not report original code.
- Any additional information required to reanalyze the data reported in this paper is available from the lead contact upon request.

EXPERIMENTAL MODEL AND STUDY PARTICIPANT DETAILS

Human study

Study participants (24±4,2 years; 184±3,2 cm; 81,5±7 kg; 7 male, 1 female) were adult white caucasian subjects with a middle-class socioeconomic status. Subjects with a male sex identified themselves as males, all subjects with a female sex identified themselves as females. All participants were healthy, physically active adolescents, which refrained from any other form of resistance exercise as disposed for the study for at least four weeks before the intervention and also during the study. All subjects were verbally and in written form informed about the study and the experimental procedures. Afterwards all subjects provided written informed consent to participate in the study. The study was approved by the ethics committee of the German Sport University of Cologne (005/2018) and all associated procedures were conducted in accordance with the Declaration of Helsinki.

Cell lines

HeLa cells (human, sex: female) were cultured in Dulbecco's modified Eagle's medium (DMEM) containing 10% fetal calf serum (FCS) and 100 U/ml penicillin as well as 100 U/ml streptomycin (PS) at 37°C and 5% CO_2.

A7r5 smooth muscle cells (embryonic rat, sex unspecified) were cultured in DMEM supplemented with 10% FCS, 4 mM L-glutamine and PS.

C2C12 and C2 myoblasts (mouse, sex: female) were cultured in high glucose DMEM containing L-glutamine, supplemented with 15% FCS, 2 mM non-essential amino acids, 1 mM sodium pyruvate and PS (proliferation medium) to a confluency of approximately 90%. Differentiation was induced by changing the medium to DMEM supplemented with 2% horse serum, 2 mM non-essential amino acids, 1 mM sodium pyruvate and PS (differentiation medium). Differentiation medium was changed every 24-48 h until extensive myotube formation was observed (day 5 for C2 cells; day 7 for C2C12).

To obtain RAB7A-L129F patient cells, a peripheral blood sample was obtained from an adult CMT2B patient of Caucasian origin, affected with a RAB7A_c.385C>T transition mutation causing a L129F missense mutation, and from an unaffected relative. The patient was diagnosed more than 20 years ago and reported by Verhoeven et al.[60] Lymphocytes were transformed with Epstein-Barr virus to obtain lymphoid cells. The lymphoid cells were revived and cultured in RPMI1640 medium, supplemented with 15% fetal bovine serum (FBS), 1% penicillin/streptomycin, 1% L-glutamine and 1% sodium pyruvate and maintained at 37°C with 6% CO_2.

Informed consent and ethical approval, in frame of the genetic and functional study of the mutation, was obtained from the local Medical Ethics Committee of the University of Antwerp (approval A00-038 of 26/01/2000).

METHOD DETAILS

Human study design

The intervention comprised of an acute exercise phase and an adaptation phase (Figure 1B). In the acute phase, participants were exposed to a significant stimulation by intense RE, which we termed standardized mechanical overload (SMO1). This was done to significantly stimulate skeletal muscle and to analyze BAG3 phosphorylation in the unadapted state. In the second phase, human subjects conducted 12 RE-sessions (twice per week for six weeks) with lower intensity to adapt skeletal muscle by repeated mechanical stimulation. At the end of the adaptation phase, we repeated the SMO procedure (SMO2) to stimulate skeletal muscle in the adapted state. Over the study, we conducted skeletal muscle biopsies before (R1 and R2) and 60 min after SMO1 and SMO2 (E1 and E2; Figure 1B). Subjects were instructed to fast overnight before biopsy-days and consume a standardized meal consisting of a nutrients-drink (Fresubin Vanille, Fresenius; 20 g protein, 24.8 g carbohydrates, 13.4 g fat, 1,260 kJ) 3 hours before biopsies. All subjects were allowed to drink water ad libitum.

Resistance exercise (RE)

The RE regimen included three different exercises:

1. Leg extensions (Gym80 Signum, Gelsenkirchen, Germany) - one set with 4, 8, and 16 repetitions of the maximum repetition range [RM] (the maximum weight which can be used to conduct just 4, 8 or 16 repetitions).
2. Leg press (MANG Sportgeräte, Bellenberg, Deutschland) - one set with 4 and 8 RM.
3. Drop jumps from a height of 60 cm - one set with 10 repetitions.

Standardized mechanical overload (SMO)

1. Leg extensions (Gym80 Signum, Gelsenkirchen, Germany) – two sets with 4, 8, and 16 repetitions of the maximum repetition range [RM] (the maximum weight, which can be used to conduct just 4, 8 or 16 repetitions). Additionally, one set of single legged eccentric leg extensions were conducted with 70% of 8 RM.
2. Leg press (MANG Sportgeräte, Bellenberg, Deutschland) - one set with 4 and 8 RM. Additionally, one set of single legged eccentric leg press was conducted with 70% of 8 RM.
3. Drop jumps from a height of 60 cm - two sets with 10 repetitions.
4. Two times downstairs stairwell walking – Each 182 stairs with a height of 18 cm, where two steps were taken at once. An elevator was used to return to the starting point.

The muscle contraction pattern and time under tension during leg extension and leg press exercises was standardized for one second concentric contraction, two seconds eccentric movement phases and 0.5 seconds for the isometric contraction at motion reversal. The inter-set rest period was 2 minutes, and the inter-exercise rest period was 3 minutes. At the beginning of each training or SMO session, a general warm-up was performed on a cycle ergometer, consisting of 5 minutes at a load of 1 W/kg body weight. This was followed by a device-specific warm-up, involving 10 repetitions with a load set at 70% of the 10 RM. The individual training weight was determined ten days before the first SMO, and this load remained constant throughout the intervention, with no progression of the weights used. All SMOs and biopsies were conducted between 8:00 AM and 11:00 AM, while the training sessions took place between 8:00 AM and 6:00 PM.

Skeletal muscle biopsies

Skeletal muscle biopsies were obtained from the midportion of the vastus lateralis muscle, using the percutaneous needle technique. The leg selected for the initial biopsy at baseline was chosen randomly. Subsequent biopsies after SMO were then taken from the contralateral leg. For repeated sampling from the same leg, a new incision was 2 cm above or below the previous sampling site. This was done to collect tissue not affected by a previous biopsy. After extraction, blood and connective tissue was carefully removed by using a scalpel or sterile swabs. Biopsy samples were then immediately frozen in liquid nitrogen and stored at -80°C for subsequent analysis. For SDS-PAGE analysis, muscle tissue was sectioned using a cryotome at -20°C, and 20 μg of each sample was placed in a pre-chilled 2 ml tube containing 2.8 mm and 1.4 mm zirconium oxide beads (CKMix – 2 ml, P000918-LYSKO-A.0, Bertin Instruments). For every milligram of muscle tissue, 30 μl of a Triton X-100-based lysis buffer was added (9803, CST), and a protease/phosphatase inhibitor cocktail (78429, Thermo Fisher) containing PMSF was added. Tissue lysis was carried out using a Precellys 24 tissue homogenizer (P000062-PEVO0-A, Bertin Instruments) with four cycles of homogenization (each 15 seconds at 5800 rpm) with a 120-second pause, during which samples were placed on ice. Following homogenization, the samples were centrifuged for 15 min at 19,640 x g at 4°C, and the supernatant was collected. Protein concentration of the samples was determined using the Pierce Bradford protein assay kit (23225, Thermo Fisher) and stored at -80°C until further use. Equal amounts of protein (12 μg) for each subject and time point were analysed by SDS-PAGE and Western blotting. Equal sample loading and transfer were checked by staining of the blot membrane with Ponceau S after transfer.

Please cite this article in press as: Ottensmeyer et al., Force-induced dephosphorylation activates the cochaperone BAG3 to coordinate protein homeostasis and membrane traffic, Current Biology (2024), https://doi.org/10.1016/j.cub.2024.07.088

Generation and validation of the anti-BAG3-pS136 antibody

The anti-BAG3-pS136 phospho-specific antibody was generated against the peptide PQRSQpSPLRG of human BAG3 (aa 131-140) and purified as described by the manufacturer using an unphosphorylated peptide (PQRSQSPLRG) (Eurogentec). Antibody specificity was verified using lysates of A7r5 cells transiently transfected with plasmid constructs for the expression of wild-type BAG3, and BAG3-S136D and BAG3-S136A mutant variants. For phosphatase treatment, cells were lysed in 50 mM HEPES, pH 7.5, 0.1 M NaCl, 2 mM DTT, 0.01% Brij35. To lysates (10 mg/ml), $MnCl_2$ (final concentration of 1 mM) and λ-phosphatase (P0753, New England Biolabs) (1,600 U/ml lysate) were added followed by incubation at 30°C for 30 min. Samples were analysed by SDS-PAGE and immunoblotting.

Electrical pulse stimulation

Differentiated C2C12 myotubes were subjected to electrical pulse stimulation (EPS) mainly as described before.[27] In brief, cells were grown on 6 well plates and electrically stimulated with a C-Pace unit (Ion Optix, Milton, MA) and a six-well C-dish electrode (Ion Optix). EPS was performed by applying pulses of 10 V for 4 ms at a frequency of 0.5 Hz ('mild EPS') or pulses of 10 V for 10 ms at 1 Hz ('twitch EPS'). Damage EPS consisted of a sequence of a 5 sec tetanic hold triggered by continuous pulses at 15 Hz, 5 sec delay, and 5 sec of pulses at 5 Hz followed by another 5 sec delay. After 5 hours of EPS treatment, cells were lysed in RIPA buffer (25 mM Tris-HCl, pH 8.0, 150 mM NaCl, 0.5% sodium deoxycholate, 1% Nonidet P-40, 0.1% SDS, 10% glycerol, complete protease inhibitor (4693132001, Roche), phosSTOP phosphatase inhibitor (4906837001, Roche)). Following sonication with 10 pulses at 100% amplitude (UP100H ultrasonic processor, Hielscher Ultrasound Technology), lysates were incubated for 20 min on ice and then centrifuged at 16,100 x g for 20 min at 4°C. Protein concentration of resultant supernatants was determined in a Bradford assay (protein assay dye, 5000006, Bio-Rad) and equal amounts of protein were analysed by SDS-PAGE and immunoblotting. Band intensities were quantified and normalised to protein amount as determined by Ponceau S staining of the blot membrane.

Unidirectional cyclic stretch

Elastomeric PDMS substrates for cyclic stretch were prepared with an elasticity of 50 kPa as described earlier.[95] For cell attachment, substrates were coated with 20 μg/ml human fibronectin (356008, Corning) in PBS for 1 h at 37°C before seeding 10,000 A7r5 cells/cm^2. Uniaxial cyclic strain was applied with a frequency of 0.3 Hz and a stretch amplitude of 20% as described earlier.[28] After stretching for 0, 0.5, 1 and 4 h cells were harvested and lysed in 30 μl RIPA buffer (89901, Thermo Fisher) per chamber supplemented with protease inhibitor cocktail (P8340, Sigma-Aldrich) and phosphatase inhibitor cocktail (P5726, Sigma-Aldrich). Crude protein extracts were centrifuged at 12,000 x g for 10 min at 4°C. The resultant supernatant was analysed by SDS-PAGE and Western blotting. Band intensities were quantified and normalised to loaded protein amount. Values obtained for the unstretched control were set to 1.

Generation and characterization of phosphosite mutant variants of BAG3

To generate BAG3 phosphosite mutant variants, site directed mutagenesis was performed by PCR using nucleotide primers with specific nucleotide substitutions and a human BAG3 cDNA as template. PCR products were subcloned into plasmid pCMV-Tag2b. All plasmids were verified by sequencing. HeLa cells were transiently transfected with the resultant plasmids using a CalPhos transfection kit (631312, Clontech), whereas A7r5 cells were transfected with JetPRIME transfection reagent (101000001, Polyplus) following the instructions of the manufacturer. 48 hours after transfection cells were collected. For immunoprecipitation of BAG3 complexes from HeLa cells, transfected cells were lysed in RIPA buffer without SDS (25 mM Tris-HCl, pH 8.0, 150 mM NaCl, 0.5% sodium deoxycholate, 1% Nonidet P-40, 10% glycerol, Complete protease inhibitor, phosSTOP phosphatase inhibitor). After 20 min of incubation on ice, the lysate was sonicated and centrifuged at 16,100 x g for 20 min at 4°C. Resultant supernatant was adjusted to a protein concentration of 10 mg/ml using MOPS/KCl buffer (20 mM MOPS-KOH, pH 7.2, 100 mM KCl, Complete protease inhibitor). Samples were incubated with M2-agarose (A2220, Sigma-Aldrich) at a concentration of 30 μl of agarose per ml of lysate for 3 h at 4°C. The agarose was collected by centrifugation at 900 x g for 1 min and was washed four times with RIPA buffer without SDS and two times with MOPS/KCl. Agarose-bound proteins were eluted using 0.1 M glycine-HCl, pH 3.5, precipitated with 12.5% trichloroacetic acid, and analysed by SDS-PAGE and immunoblotting.

To monitor impact of BAG3 phosphosite mutant variants on CASA activity, A7r5 cells were seeded on human fibronectin (1.25 μg/cm^2; F2006, Sigma-Aldrich) coated culture dishes. 24 h after seeding cells were transiently transfected with plasmid constructs for mutant variant expression and further grown for 48 h. 3 hours prior to lysis cells were treated with 50 μM cycloheximide (8682.1, Roth) to inhibit protein synthesis. Cells were lysed in RIPA and further analysed as described above. After SDS-PAGE and immunoblotting, SYNPO2 isoforms targeted by BAG3 for autophagic degradation were quantified and ratios of protein levels in the presence and absence of CHX were determined.

Proteome preparation and mass spectrometry

To isolate FLAG-BAG3 complexes for mass spectrometry, five 10 cm culture dishes of A7r5 cells were cultivated per condition and grown to ~60% confluency prior to transfection with FLAG-BAG3 variants-encoding pCMV-Tag2b plasmids with JetPRIME transfection reagent according to the protocol of the manufacturer (101000001, Polyplus). 32 hours after transfection, cells were collected, washed with PBS, and resuspended in RIPA buffer without SDS (25 mM Tris-HCl, pH 8.0, 150 mM NaCl, 0.5% sodium deoxycholate, 1% Nonidet P-40, 10% glycerol, Complete protease inhibitor, phosSTOP phosphatase inhibitor). Following sonication with 10 pulses at 100% amplitude (UP100H ultrasonic processor, Hielscher Ultrasound Technology), lysates were incubated for 20 min on ice and

then centrifuged at 16,100 x g for 20 min at 4°C. The resultant supernatant was adjusted with IP buffer (20 mM MOPS, pH 7.2, 100 mM KCl) to a protein concentration of 5 mg/ml. To 5 mg of lysate 15 μl of anti-FLAG magnetic beads (A36797, Thermo Fisher) were added. After incubation on a rotating wheel for 1.5 hours at 4°C, beads were collected in a magnetic field and washed 5-times with 1 ml of IP buffer containing 0.1% Tween 20, followed by one washing with IP buffer. Bound material was eluted by incubation in 50 mM HEPES, pH 7.5, 2% SDS (proteomics grade; M112, VWR) at 95°C for 5 min.

Immunoprecipitation eluates were reduced with 10 mM DTT at 37°C for 30 min and alkylated with 50 mM chloroacetamide at room temperature (RT) in the dark for 30 min. Alkylation was quenched with 50 mM DTT at RT for 20 min. Proteins were purified using SP3 beads, resuspended in 50 mM HEPES, pH 7.4, 5 mM $CaCl_2$ buffer and Trypsin (Serva) added at 1:100 (w/w) protease to proteome ratio, and incubated shaking at 37°C for 18 h. Digested peptides were de-salted using self-packed C18 STAGE tips and resuspended in 0.1% formic acid in water. For each sample, 1 μg desalted peptides were loaded on an Ultimate 3000 RSLC nano chromatography system (Thermo Fisher), with a μPAC reverse phase trap column (COL-TRPNANO16G1B2, Thermo Fisher) and a 50 cm μPAC reverse phase analytical column (COL-NANO050G1B, Thermo Fisher), operated at 40°C. Samples eluted using 600 nl/min flow rate and a 90 min binary gradient from 1-30% eluent B (A: 0.1% formic acid in water, B: 0.1% formic acid in acetonitrile), 2 h total time. Separated peptides were ionized using a Captive Spray ion source (Bruker) into an Impact II Q-TOF mass spectrometer (Bruker). The HyStar Software (v3.2, Bruker) was used for data dependent acquisition in the 200–1750 *m/z* range with MS1 spectra acquisition rate of 4 Hz and the top 17 most intense ions selected for fragmentation. Fragmented precursors ions were excluded from repeated analysis for 30 s unless signal to noise ratio improved >3-fold. Fragmentation spectra were acquired between 5 Hz for low-intensity (>500 cts) and 20 Hz for high intensity (>5k cts) precursors, with stepped parameters, each with 50% acquisition time dedicated to each precursor: 100 μs transfer time, 7 eV collision energy, and collision radio frequency (RF) of 1500 volt peak to peak (Vpp), followed by 100 μs transfer time, 9 eV collision energy and collision RF of 1700 Vpp.

Proteome data analysis

MaxQuant (v.2.0.3.0)[90] was used for peptide identification from the acquired mass spectrometry data, using standard settings for Bruker Q-TOF instruments. FASTA files containing *Rattus norvegicus* UniProt protein sequences, human BAG3 wild type and mutant sequences, and appended standard contaminants were used for database searches applying false discovery rate (FDR) cutoffs of 0.01 at the level of peptide-sequence-matching (PSM) and protein identification. Label-free quantification (LFQ) and "match between runs" were enabled. Trypsin was set as digestion enzyme, oxidation (M) and acetylation (protein N-term) as variable modifications and cysteine carbamidomethylation as fixed modification. Three replicates of the empty control and two replicates of IPs with AA variant were excluded after initial analysis due to low number of peptide identifications (less than 50% of average background binding in empty samples) which compromised LFQ comparison. LFQ data was analysed using Perseus (v2.0.10.0), filtering proteins quantified in $\geq$ 60% replicates in at least one condition followed by imputation of missing values with standard settings. Principal component analysis was performed on proteins with significant differences in abundance (ANOVA p-value < 0.05 with Tukeyś Post-hoc test FDR < 0.05). Differential Expression (DE) statistical analysis was performed using LIMMA R package plugin within Perseus.[91] BAG3 interactors were determined by filtering for proteins significantly enriched (LIMMA-moderated t-test p-value < 0.05) in pulldowns with at least one human BAG3 variant compared to control. Heatmaps and Volcano plots were produced in R using ComplexHeatmaps[92] and EnhancedVolcano (https://github.com/kevinblighe/EnhancedVolcano) respectively. Gene Ontology (GO) enrichment analysis was performed with ShinyGO.[93] See Table S1, Data S1 and Data S2 for more information.

Monitoring autophagic degradation following RNA interference

To elucidate a role of HSPB1 in CASA, rat A7r5 cells were grown to about 30% confluency on fibronectin, medium was exchanged, and cells were transfected with control siRNA (Mission siRNA universal negative control, Sigma-Aldrich) or siRNA directed against HSPB1 (siHSPB1), respectively (Mission siRNA, Sigma-Aldrich) using JetPRIME transfection reagent. For each sample, corresponding to a 10 cm cell culture plate with 10 ml medium, 6 μl siRNA (20 μM stock), 8 μl JetPRIME reagent, and 200 μl JetPRIME buffer were used. 16 hours after transfection medium was exchanged. 41 hours after transfection cells were treated with BafA1 (100 nM; sc-201550A, Santa Cruz Biotechnology) for 7 hours prior to cell lysis and analysis by SDS-PAGE and immunoblotting.

The role of RAB proteins in CASA was analysed in mouse skeletal muscle cells. C2 myoblasts were grown in proliferation medium. When cells reached ~70% confluency, medium was exchanged to differentiation medium and cells were transfected with control siRNA (Mission siRNA universal negative control, Sigma-Aldrich) or siRNA directed against RAB2A, RAB11A, and RAB7A, respectively (Mission siRNA, Sigma-Aldrich) using JetPRIME transfection reagent. Final concentration of siRNAs was 60 nM. After 24 hours medium was exchanged. On the second day of differentiation siRNA transfection was repeated. On the fifth day of differentiation cells were treated with BafA1 (300 nM; sc-201550A, Santa Cruz Biotechnology) for 5 hours prior to cell lysis and analysis by SDS-PAGE and immunoblotting.

Autophagosome formation and maturation assay

A7r5 cells grown on fibronectin were transfected with plasmids mCherry-EGFP-LC3B and pcDNA3.1-RAB7A-T22N using the JetPrime transfection kit. For this approach, the RAB7A-T22N coding region had been subcloned from plasmid pEGFP-C1-Rab7A-T22N[96] into vector pcDNA3.1, Control cells were transfected with mCherry-EGFP-LC3B and empty pcDNA3.1. 48 h after transfection, cells were fixed with 4% paraformaldehyde/phosphate-buffered saline for 15 min at 37°C, followed by 3 washing steps with PBS. The cells were mounted in Fluoromount-G (00-4958-02, Thermo Fisher) and subjected to fluorescence microscopy using a

Zeiss confocal laser scanning microscope equipped with a Plan-Apochromat 63x/1.40 Oil DIC objective (LSM710, AxioObserver) or a Zeiss Cell Observer SD spinning disk microscope equipped with an alpha Plan-Apochromat 63x/1.46 Oil Korr M27 objective (Axio Observer.Z1/7). Obtained confocal images were subjected to manual counting of autophagosomes and autolysosomes using the multi-point tool of ImageJ. Autophagosomes and autolysosomes were identified as such when they could be differentiated from the background as distinct puncta. The same photographs were subsequently used to manually quantify the cell area by outlining the perimeter of the cells using the freehand selection tool of ImageJ.

In-vitro binding assays

The cDNA encoding BAG3-T285A/S289A was subcloned into plasmid pET-M11. The plasmid construct and a construct encoding wild-type BAG3,[16] respectively, were used for expression of His-tagged BAG3 variants in *E. coli* BL21(DE3) and subsequent purification of the tagged protein on Ni-NTA-agarose as described by the manufacturer (30210, Qiagen). For expression of His- and T7-tagged RAB7A, the coding region of RAB7A was subcloned from plasmid pEGFP-C1-Rab7A[96] into pET-28a, followed by expression in BL21(DE3) cells and purification on Ni-NTA-agarose. Similarly, LC3B was expressed and purified after subcloning of the LC3B coding region from plasmid mCherry-EGFP-LC3B[89] into vector pET23-EEF.[87] Purified proteins were mixed at a concentration of 1 μM each in 20 mM MOPS, pH7.2, 100 mM KCl, and 0.1% Tween 20 (incubation buffer). Buffer contained in addition 10 mM EDTA, 2 mM GDP (20-177, Merck), or 0.2 mM GTP-γ-S (20-176, Merck) when indicated. For pulldown of RAB7A complexes, samples (50 μl) received 1 μg anti-T7-tag antibody together with 6 μl of protein-G-sepharose (GE17-0618-01, Sigma-Aldrich). After incubation for 1 h at 4°C, sepharose beads were collected by centrifugation at 900 x g for 1 min. Beads were washed 3 times with incubation buffer and once with incubation buffer without Tween 20. Isolated complexes were eluted with 0.1 M glycine-HCl, pH 3.5, precipitated with 12.5 % trichloroacetic acid, and analysed by SDS-PAGE and immunoblotting.

Analysing BAG3 dephosphorylation upon mitophagy induction

Following 5 days of differentiation, C2 myotubes were treated for 16 hours with 10 μM CCCP (C2759, Sigma-Aldrich) or 1 μM valinomycin (94675, Sigma-Aldrich). Cells were collected and lysed, followed by lysate analysis by SDS-PAGE and immunoblotting.

Cultivation and analysis of CMT2 patient cells

Lymphoid cells from a RAB7A-L129F patient and an unaffected relative were analysed to investigate the impact of the disease mutation on CASA activity. Mutant and healthy control-derived cells, respectively, were equally divided in T25 flasks in duplicates with fresh medium. Lymphoid cells were exposed to either 0.01% DMSO or 100 nM BafA1. After 7 hours, cells were collected in centrifugation tubes, supernatant was removed, and the cell pellets were washed in ice-cold PBS before lysis in RIPA buffer (25 mM Tris-HCl, pH 8.0, 150 mM NaCl, 0.5% sodium deoxycholate, 1% Nonidet P-40, 0.1% SDS, 10% glycerol, complete protease inhibitor (4693132001, Roche), phosSTOP phosphatase inhibitor (4906837001, Roche)). Following sonication with 10 pulses at 100% amplitude (UP100H ultrasonic processor, Hielscher Ultrasound Technology), lysates were incubated for 20 min on ice and then centrifuged at 16,100 x g for 20 min at 4°C. Protein concentration of resultant supernatants was determined in a Bradford assay (protein assay dye, 5000006, Bio-Rad) and equal amounts of protein were analysed by SDS-PAGE and immunoblotting. Band intensities were quantified and normalised to protein amount as determined by Ponceau S staining of the blot membrane.

QUANTIFICATION AND STATISTICAL ANALYSIS

Quantification of blot lane intensities was performed using ImageJ. Values were normalised for loaded protein amount deduced by Ponceau S staining or by immunoblotting with anti-γ-tubulin antibody (T5326, Sigma-Aldrich). Data were analysed for statistical significance using GraphPad prism 10. The number of independent experiments and the used statistical test is specified in the figure legends.